AD-A063 934 AIR FORCE INST OF TECH WRIGHT-PATTERSON AFB OHIO SCH--ETC F/G 18/3
THE NUCLEAR AIR-SHOCK PRECURSOR: A STUDY OF THE CONTRIBUTION OF--ETC(U)
DEC 78 R N PRICE

UNCLASSIFIED AFIT/GNE/PH/78D-21 NL

1 OF 2
AD A063934

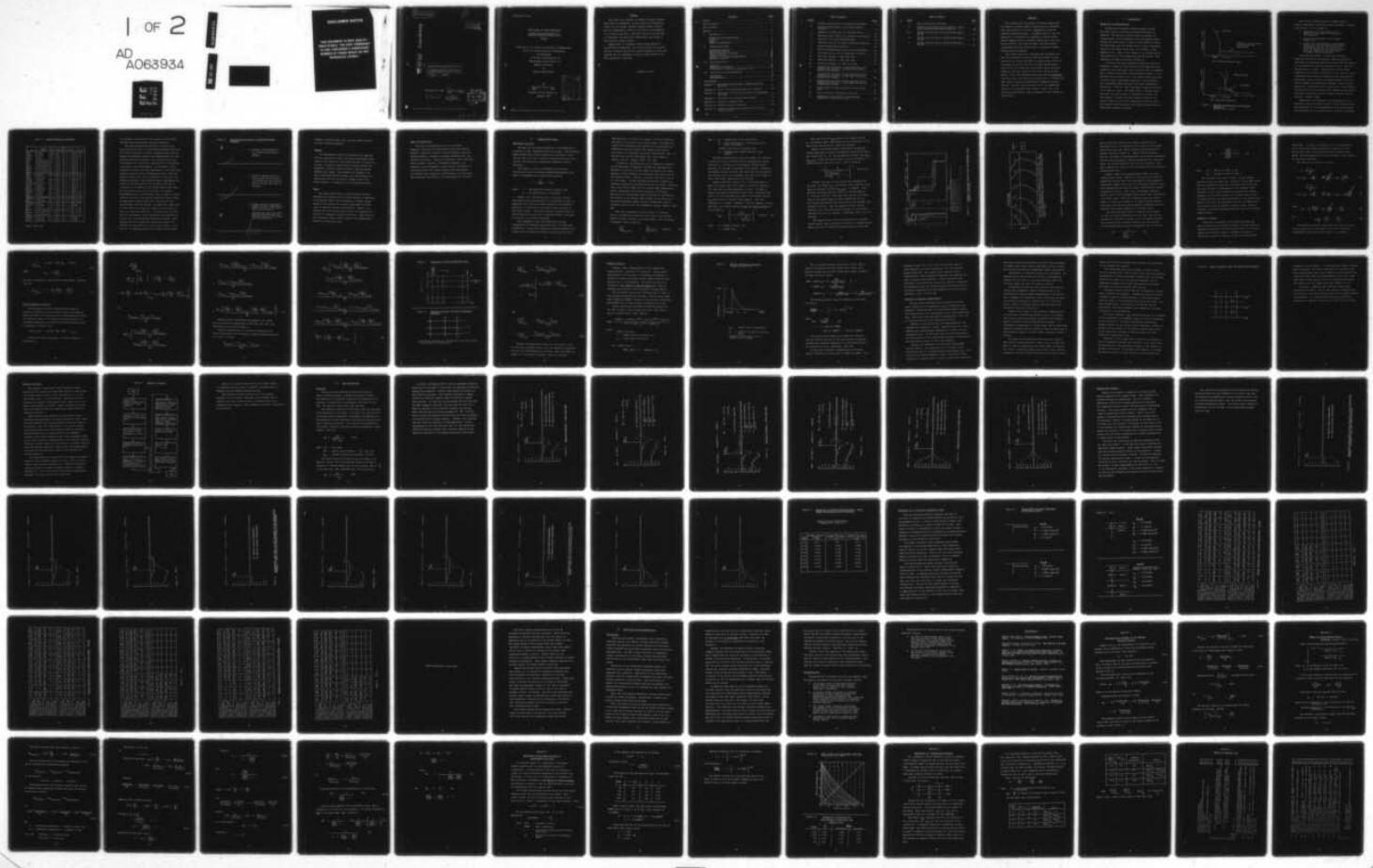

(14) AFIT/GNE/PH/78D-21

(1)

LEVEL II

AD A063934

DDC FILE COPY

(6) THE NUCLEAR AIR-SHOCK PRECURSOR:
A STUDY OF THE CONTRIBUTION OF
AIRBLAST-GENERATED SEISMIC WAVES.

(9) Master's THESIS,

(10) Richard N. Price
Capt USAF

AFIT/GNE/PH/78D-21

(11) Dec 78

(12) 112 p.

Approved for public release; distribution unlimited

012 225

AFIT/GNE/PH/78D-21

THE NUCLEAR AIR-SHOCK PRECURSOR: A STUDY OF THE CONTRIBUTION OF AIRBLAST-GENERATED SEISMIC WAVES

THESIS

Presented to the Faculty of the School of Engineering

of the Air Force Institute of Technology

Air University

in Partial Fulfillment of the

Requirements for the Degree of

Master of Science

in

Nuclear Engineering

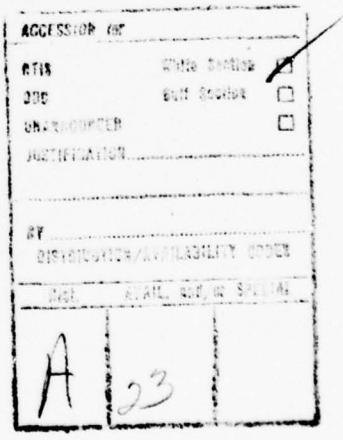

by

Richard N. Price, B.A.
Capt USAF

Graduate Nuclear Engineering

December 1978

Approved for public release; distribution unlimited

Preface

This thesis was intended to determine whether airblast energy from an atmospheric nuclear burst could effectively couple into the ground, generate surface seismic signals, and thus independently cause or contribute to the formation of an airshock precursor. The major thrust of the work was to investigate the generation, description, and timing of these surface seismic signals.

Appreciation is extended to Major George Nickel of the AFIT Physics Department for his recognition of an effort worthy of research and for his earnest attempts to teach free thinking and the independent analytical application of the first principles of physics.

Richard N. Price

Contents

List of Figures

List of Tables

Abstract

The coupling into the ground of airblast energy from an atmospheric nuclear burst is postulated as a mechanism which may contribute to if not independently cause the observed airshock precursor. A computer model to test the hypothesis is constructed by assuming an elastic ground medium, applying finite difference techniques to the equations of motion, and using the space- and time-varying overpressure from the nuclear burst to induce the seismic motions within the ground.

The surface velocities resulting from simulation of a 28 kiloton atmospheric burst at 500 feet height of burst yielded a dust layer ballistically reaching only 0.64 cm at its highest point for the stiff one-layer ground medium, 0.096 cm for the softer one-layer medium, and a negligible height for the more realistic four-layer Frenchman Flats medium. Thus, the airblast-induced precursor as postulated (ballistic rise only) fails to re-create the 2 - 3 meter high dust layers observed in experimental atmospheric nuclear testing. However, the motions are felt to be significant enough to be included in any attempt to model from first principles the precursor and the up-sweep of dust behind the shock front.

I. Introduction

Background and Phemonenology

During early atmospheric nuclear weapons testing the effect known as the nuclear airblast precursor was observed. The precursor results from the formation of a heated layer of air immediately above the ground surface. Because the sound speed is higher in this heated air layer, the shock front from the nuclear burst is able to propagate faster in this heated region than in the higher, cooler regions of air. Thus, a "toe" forms on the leading edge of the shock front at its intersection with the ground. This phenomenon is shown pictorially in Figure 1.

A nuclear burst which generates an airblast precursor represents a departure from the shock front shape and shock properties one would expect when a nuclear burst is detonated over an ideally reflecting, non-interacting surface. It is precisely the interaction of a real surface which gives rise to the non-ideal (precursed) properties of the airblast: two overpressure peaks instead of one; peak overpressure reduced up to 50% over ideal; and dynamic pressure increased up to 100% over ideal. The properties of a nuclear blast precursor therefore become of considerable interest when the response of surface and near-surface systems to the static loading of real-world overpressure waveforms and to the enhanced drag loading from the dynamic pressure must be known with reasonable accuracy.

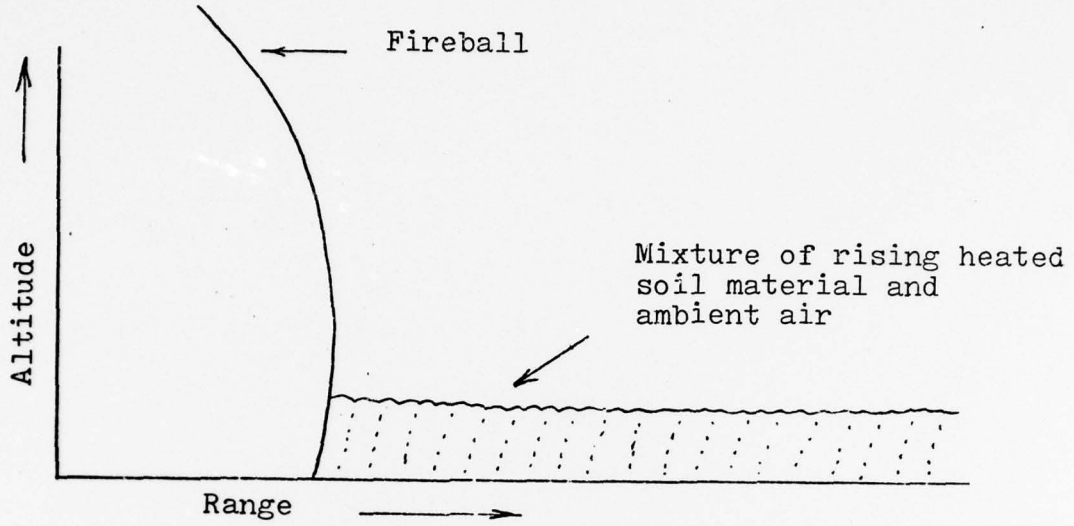

(a) Pre-Shock Thermal Layer

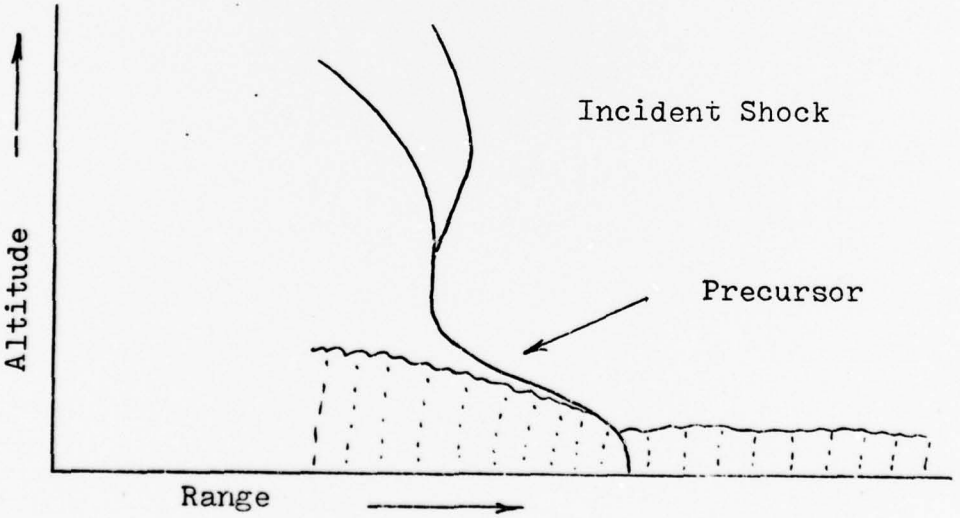

(b) Blast-Wave Precursor

Figure 1. Pictoral Representation of Precursor Phenomenon
(Knasel, 1975: 2.15)

The Air Force Weapons Laboratory (AFWL) began to study the precursors observed in actual atmospheric nuclear tests (Table I) in an attempt to

1. characterize the development of the heated air layer which is the heart of the precursor;

2. model the development of this thermal region; and

3. extend this understanding of experimental observations for the relatively low yield experimental nuclear blast precursors (1 to 30 kilotons) to the megaton yields which the defense planner must expect in today's threat environment.

Utilizing considerable internal and contractor expertise from 1973 to the present, AFWL has principally concluded that radiation (primarily X-rays) from the fireball is the mechanism by which the heated air layer (and thus the precursor) is formed. Specifically, if the thermal radiation on the ground is sufficient to heat the soil above a threshold level (which will depend on soil type and soil conditions), ground moisture and hydrated water in the soil will be suddenly and explosively released. Such a violent release will "popcorn" the soil into the air. Once airborne, the dust heats the surrounding air by conduction and convection while continuing to absorb thermal radiation from the fireball. (Ganong, 1978)

Nonetheless, the coupling of airblast energy to the ground has been postulated as another causal mechanism which may contribute to if not independently cause the precursor. This mechanism has not been previously studied to determine

Table I. Events Studied for Precursor

Shot	Operation (Number)	Yield (Kt)	HOB (ft)	Scaled HOB ($ft/Kt^{1/3}$)	Area at NTS	Type	Precursor*
POST	Teapot (11)	1.45	300	265	9	Tower	Yes
MOTH	Teapot (2)	2.40	300	224	3	Tower	Yes
HORNET	Teapot (5)	3.6	300	196	3	Tower	Yes
TESLA	Teapot (3)	6.8	300	158	9	Tower	Yes
FOX	Tumbler-Snapper (6)	11.5	300	133	4	Tower	?
EASY	Tumbler-Snapper (5)	12.5	300	129	1	Tower	?
HOW	Tumbler-Snapper (8)	13.9	300	125	3	Tower	?
NANCY	Upshot-Knothole (2)	24	300	104	4	Tower	?
BADGER	Upshot-Knothole (6)	25	300	103	2	Tower	?
HARRY	Upshot-Knothole (8)	32.3	300	94	2	Tower	?
SIMON	Upshot-Knothole (7)	45	300	84	1	Tower	?
MET	Teapot (12)	22.5	400	142	FF	Tower	Yes
BEE	Teapot (6)	8	500	250	7	Tower	Yes
MORGAN	Plumbbob (30)	8	500	250	9	Balloon	Yes
WILSON	Plumbbob (5)	10.3	500	230	9	Balloon	Yes
KEPLER	Plumbbob (11)	10.3	500	230	4	Tower	No
BOLTZMANN	Plumbbob (2)	11.5	500	222	7	Tower	?
APPLE I	Teapot (8)	14.2	500	206	4	Tower	Yes
SHASTA	Plumbbob (16)	16.5	500	196	2	Tower	No
WHITNEY	Plumbbob (28)	18.5	500	189	2	Tower	?
ZUCCHINI	Teapot (14)	28	500	165	7	Tower	Yes
APPLE II	Teapot (13)	28.5	500	164	1	Tower	Yes
TURK	Teapot (4)	44	500	142	2	Tower	Yes
GRABLE	Upshot-Knothole (10)	15	524	212	FF	Gun	Yes
PRISCILLA	Plumbbob (6)	36.6	700	211	FF	Balloon	Yes
SMOKY	Plumbbob (20)	44	700	198	8	Tower	Yes
WASP PRIME	Teapot (9)	3.2	739	502	7	Air	Yes
LA PLACE	Plumbbob (24)	1.22	750	702	7	Balloon	?
WASP	Teapot (1)	1.2	762	717	7	Air	No
ABLE	Tumbler-Snapper (1)	1	793	793	FF	Air	No
DOG	Tumbler-Snapper (4)	18.5	1040	393	7	Air	Yes
CHARLIE	Buster-Jangle (3)	14	1132	470	7	Air	Yes
CLIMAX	Upshot-Knothole (11)	60	1334	341	7	Air	Yes
DOPPLER	Plumbbob (17)	10.7	1500	681	7	Balloon	?
NEWTON	Plumbbob (26)	11.8	1500	659	7	Balloon	?
STOKES	Plumbbob (14)	19	1500	562	7	Balloon	?

(Liner, 1975: 22)

its relative contribution to the heated air layer which precedes and determines the precursor formation.

The airblast-generated precursor contribution as postulated would occur in the following sequence (Figure 2): the airblast strikes the ground, coupling energy into the ground and generating seismic-like displacements; the displacement waveforms propagate into the ground along the soil surface with velocities characteristic of the seismic velocities of the ground medium. As the radius of the airshock increases, the peak overpressure at the shock front decreases and the airshock subsequently slows. When the seismic surface wave velocity exceeds the velocity of the advancing airblast, these seismic surface disturbances will outrun the airshock and are for the first time able to contribute to the thermal layer formed ahead of the shock. For this contribution to be of concern, the surface disturbances must be sufficiently large to impart a sizable vertical velocity to the dust/soil particles lying loosely on the ground, causing these loose particles to rise ballistically above the ground. One additional requirement is that sufficient energy must remain in the fireball to heat the rising dust particles. The heated dust can then heat the surrounding air by conduction and convection as in the case of the thermally-induced soil blowoff. Early heating from the fireball will practically assure the presence of loose, dry soil at the ground surface. As in the case of thermally-induced soil blowoff, the airblast-

Figure 2. Pictoral Representation of Airblast-Induced Precursor

a. Airblast strikes ground at T_o; Fireball heats ground surface.

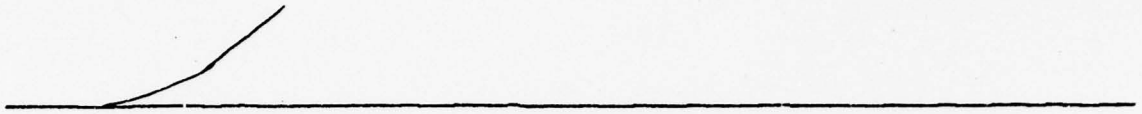

b. Airblast expands along surface; Seismic waves radiate into ground and along surface but move slower than front of airshock.

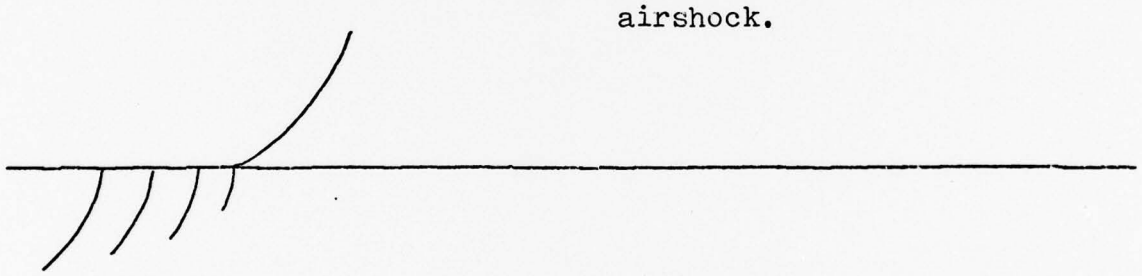

c. Seismic waves are now able to outrun airblast, imparting an upward velocity to dust particles on the surface;

Injected dust particles absorb fireball radiation and heat the surrounding air by conduction and convection.

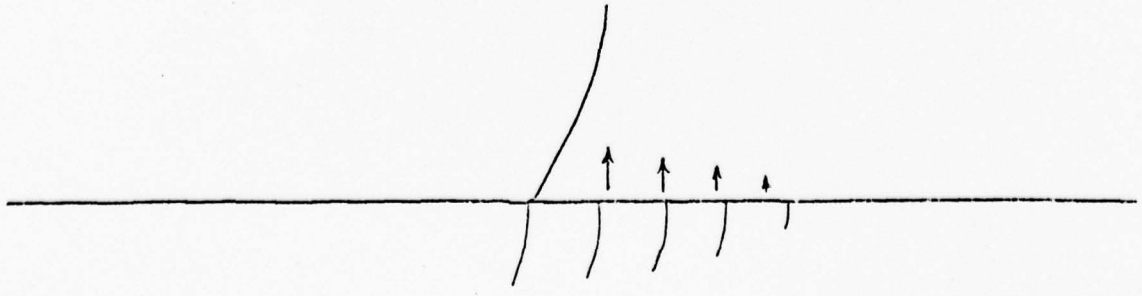

induced contribution will also be yield, height of burst, and soil condition dependent.

Purpose

The documentation which follows details the approach that was undertaken to model any airblast-generated contribution to the heated air layer which precedes the precursor. As such, it presents computations of seismic surface displacements, seismic surface velocities, and anticipated airborne dust layers. This research is intended to be used to determine whether further, more exact modeling is warranted on the role of airblast energy couples into seismic waves as a contributor to the nuclear precursor.

Scope

The computational model to simulate ground motions developed as a product of this thesis research is applicable to any problem which involves pressure or stress loading normal to the surface of an elastic half-space for which order of magnitude answers are desirable. However, the problems for which ground motion results are presented are limited to atmospheric nuclear test events. This work does not investigate thermal energy transport or hydrodynamics within the rising dust layer.

Order of Presentation

The order of presentation will be as follows: Chapter II describes the computational model (preliminary analysis, equations of motion, finite difference equations, surface pressure, treatment of boundary displacements, and method of solution); Chapter III discusses output calculated from the model (stability, transmitting boundary, and simulation of an atmospheric nuclear burst); and Chapter IV concludes whether the seismic surface waves generated by the airblast make significant contributions to the precursor and recommends improvements or new approaches for the model.

II. Computational Model

Preliminary Analysis

The heart of the airblast precursor is the formation of a heated air layer immediately above the ground. The postulated means through which seismic signals can contribute to this thermal layer is by the injection of dust/soil particles into the air, these particles subsequently absorbing fireball radiation.

The height h to which a dust particle would rise ballistically above the surface (ignoring hydrodynamics and drag) is independent of its mass and is given by

$$h = \frac{v^2}{2g} \quad \text{(cm)},$$

where v = the particle's vertical velocity, and

g = the gravitational acceleration.

Clearly then, the driving force involved in testing this postulated causal mechanism is to calculate an order of magnitude value for the vertical velocity of the dust/soil particles, or equivalently, the peak vertical velocity of the ground surface. The single greatest assumption made is that satisfactory values can be obtained through a treatment of the soil as an elastic half-space.

This assumption is put into perspective through consideration of research conducted by the U. S. Army Corps of Engineers. Since 1971 computations and data analyses have simulated and reconstructed seismic motions resulting from

high explosive and nuclear test events. This work indicates that while soils are not truly elastic media, two-dimensional elastic wave propagation calculations can be performed with comparative ease and require only limited soil property data relative to inelastic, non-linear calculations. Also, it was felt that elastic calculations were less subject to numerical errors. (Hadala, 1973: 297, 383)

In addition, one particular set of computations compiled by the Army Corps of Engineers revealed that for peak overpressures in the 100 to 50 psi range, the elastic soil model generally yielded maximum velocities less than those given by the inelastic model. However, the reverse was true in the 50 to 1 psi range. In other related calculations a similar but different overpressure crossover point was also found. Generally then, these results imply that the elastic model subsequently used to approximate the vertical velocities of the dust particles will underestimate these velocities if outrunning of the airshock by the seismic signal occurs at the high end of the peak overpressure region and will overestimate them if outrunning occurs in the low overpressure region. (Hadala, 1973: 295)

After first assuming an elastic medium, an estimate through one-dimensional analysis can be made of the maximum surface vertical velocity in a uniform media. This is derived in Appendix A and is given by

$$\left(\frac{d\,S_z}{dt}\right)_{\max \text{ at } z=0} = \frac{P_o}{\rho_{\text{ground}}\, V_c} \quad \text{(cm/sec)}, \qquad \text{(1a)}$$

where S_z = displacement in the z-direction,

P_o = peak overpressure on the surface at the point of interest,

ground = density of the ground, and

V_c = compressional seismic velocity of the ground.

The peak overpressure P_o along the surface is a function of yield and height of burst; and the compressional seismic velocity V_c is a function of the seismic constants (Lamé constants λ and μ) and density of the ground. Therefore, the maximum vertical velocity with which dust can be injected into the air will also be dependent upon the yield, height of burst, and seismic properties of the ground.

Another important consideration - the ground range at which the seismic signal will begin to outrun the airshock - will also have the same dependency as above. In order to obtain a preliminary estimate of where this "outrunning" will occur, it is first assumed that there is an average velocity V_{ave} with which the sperical shock expands. With this assumption it is shown in Appendix G that the apparent velocity with which the airshock advances along the ground surface can be expressed as

$$V_{app} = \left\{ \frac{V_{ave}^2}{1 - \frac{H^2}{H^2 + r^2}} \right\}^{\frac{1}{2}} \quad \text{(cm/sec)} \quad (1b)$$

where H = height of burst, and

r = ground range.

When this velocity V_{app} slows to the seismic velocity V_c, the seismic signal thus created at the intersection of the shock front and ground will outrun the airshock.

However, the surface seismic disturbances having the largest magnitude are known to be Rayleigh waves which travel more slowly than V_c. So, solving Equation 1b for r when $V_{app} = V_{Rayleigh}$, yields that ground range at which outrunning of seismic Rayleigh waves will occur. This is given by

$$r \geq \left\{ \frac{H^2}{\left[\frac{V_{Rayleigh}}{V_{ave}} \right]^2 - 1} \right\}^{\frac{1}{2}} \quad \text{(cm or ft).}$$

Consider the case of a 30 kiloton burst detonated at 500 feet, also where V_{ave} = 2.4 km/sec (eight times the sound speed in sea-level air) and $V_{Rayleigh}$ = 2.5 km/sec. Then, Rayleigh outrunning begins to occur at a ground range of r = 0.52 km = 1714 ft. From blast data curves it is found that at that ground range the peak overpressure will be $P_o \cong 40$ psi and that the time of arrival of the airshock will be TARR $\cong$ 0.15 sec. Thus the maximum vertical velocity (Equation 1a) is 2.6 cm/sec and 50 percent of the fireball radiation has yet to be emitted. (Glasstone, 1977: 111, 121, 309-310)

While Equations 1a and 1b were derived for a uniform elastic medium, peak velocities occurring in a layered elastic medium are also of interest because ground motion data and

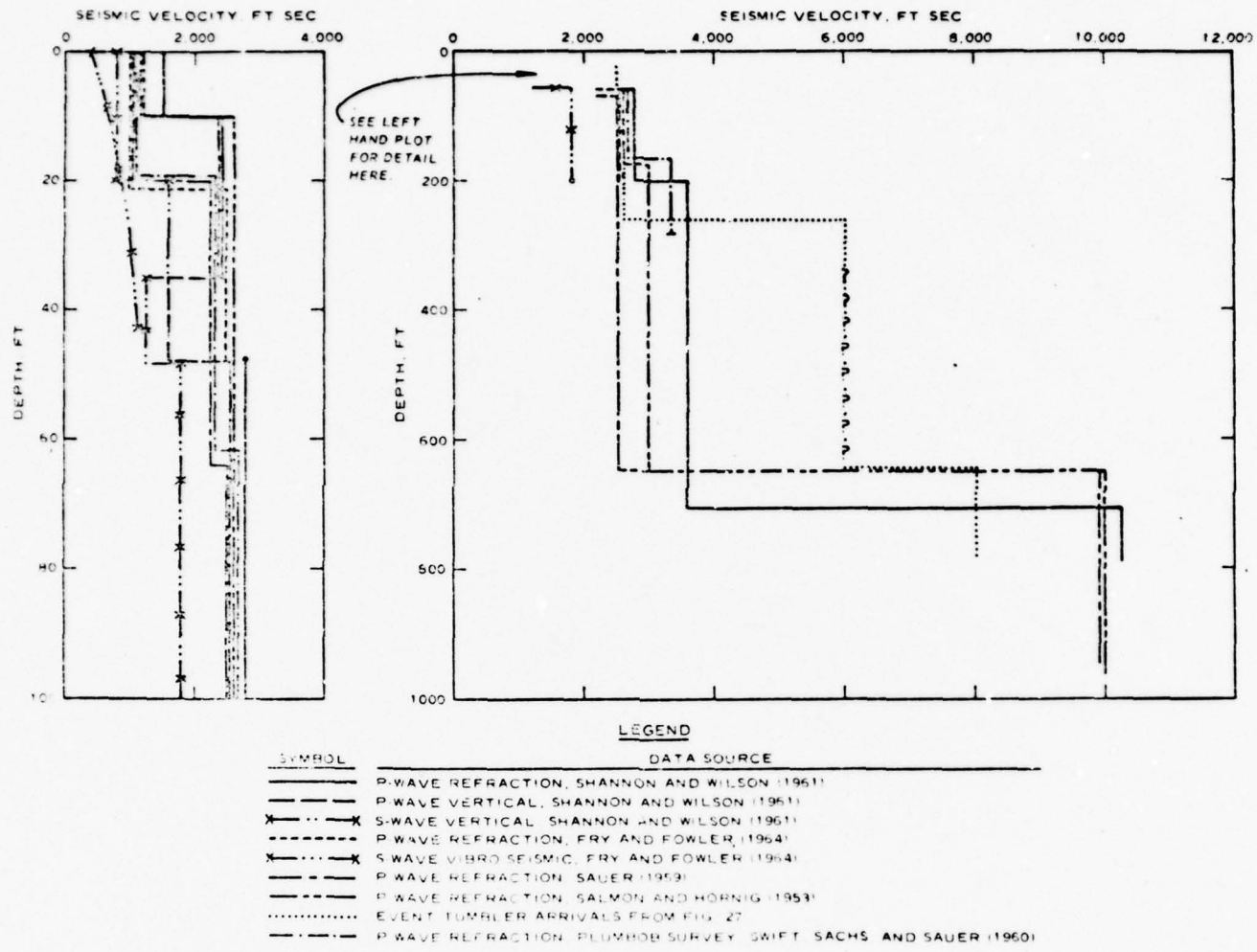

Figure 3. Summary of Seismic Velocity Data for Frenchman Flats (Hadala, 1973: 103)

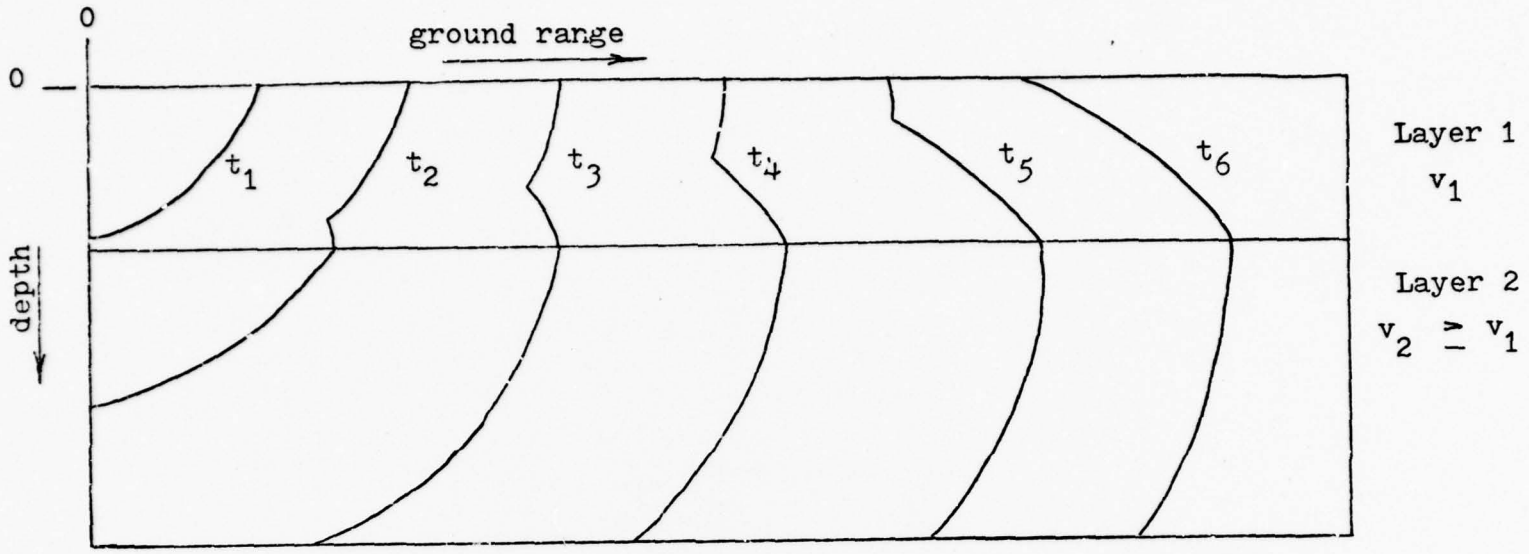

This figure depicts the propagation of a seismic wave. By time t_6 the disturbance at the ground surface is being caused by the refracted/reflected signal from the lower, seismically faster layer.

Figure 4. Phenomenological Effect of a Layered Ground Medium (Hadala, 1973: 145)

soil testing have revealed that testing grounds such as Frenchman Flats at the Nevada Test Site consist of horizontal layers which vary with depth in density and characteristic seismic velocities (Figure 3). Because elastic property data for the medium at Frenchman Flats are known and atmospheric nuclear tests displaying an airblast precursor were conducted there, the layered medium of this site will provide a "real-world" problem with which to test the postulate of the airblast - generated precursor.

Figure 4 depicts the phenomological effect of a two-layered ground medium. Typically, because of the effects of weathering, pressure from the overburden, and some degree of cementation, deeper layers will be seismically "stiffer" (read less compressive) and possess a higher characteristic seismic propagation velocity. Thus, once a disturbance reaches a stiffer layer it will propagate more quickly than a disturbance in an above layer. This will ultimately cause the seismic signal to outrun the airblast at the ground surface earlier than would have occurred had the material consisted solely of material with seismic properties of the upper layer.

One other important effect of layering in the medium is that the stress transmitted into the lower layer can be greater than the stress incident on the interface from above. The transmitted and reflected stresses have been derived from one-dimensional analysis in Appendix B and are given by

$$\sigma_t = \frac{2}{\frac{\rho_1 c_1}{\rho_2 c_2} + 1} \sigma_i$$

and

$$\sigma_r = \frac{\frac{\rho_2 C_2}{\rho_1 C_1} - 1}{\frac{\rho_2 C_2}{\rho_1 C_1} + 1} \sigma_i ,$$

where ρ_j = density of layer j, and

C_j = seismic velocity of layer j.

For a stiffer lower layer, density ρ_2 and seismic velocity C_2 will be larger than ρ_1 and C_1 of the upper layer. Thus the transmitted stress will be greater than and of the same type (tensile or compressive) as the incident stress. Therefore, if the energy attenuation resulting from spatial expansion of the seismic signal is not greater than the gain in stress achieved, the stress transmitted to the second layer which is then later re-transmitted back into the upper layer can be greater than the original incident stress, thereby resulting in seismic displacements greater than in the single-layered medium.

Equations of Motion

Armed with a knowledge of the seismic phenomenology and the parameters upon which it depends, the next step is to generate the equations which govern the motion of the ground medium under airblast loading. Cylindrical geometry is chosen due to the axial symmetry of the advancing airblast

shock front. S_r and S_z are defined to be the displacements in the radial and vertical directions, respectively. of a given point within the ground medium about its equilibrium point. The displacement S_θ in the θ-direction is zero because of the problem symmetry.

The equations of motion are given by

$$\rho \frac{\partial^2 S_r}{\partial t^2} = (\lambda + 2\mu) \frac{\partial \Delta}{\partial r} - \frac{2\mu}{r} \frac{\partial \bar{\omega}_z}{\partial \theta}^{0} + 2\mu \frac{\partial \bar{\omega}_\theta}{\partial z} \tag{2}$$

$$\frac{\partial^2 S_z}{\partial t^2} = (\lambda + 2\mu) \frac{\partial \Delta}{\partial z} - \frac{2\mu}{r} \frac{\partial}{\partial r} (r \bar{\omega}_\theta) + 2\mu \frac{\partial \bar{\omega}_r}{\partial \theta}^{0} \tag{3}$$

where

$$\Delta = \frac{1}{r} \frac{\partial (r S_r)}{\partial r} + \frac{1}{r} \frac{\partial S_\theta}{\partial \theta}^{0} + \frac{\partial S_z}{\partial z} , \tag{4}$$

and

$$2 \bar{\omega}_\theta = \frac{\partial S_r}{\partial z} - \frac{\partial S_z}{\partial r} . \tag{5}$$

The boundary conditions which apply are that the stress at the surface z=0 in the vertical direction is just the overpressure P(r,t) which acts normal to the surface.

$$\sigma_{zz}\Big|_{z=0} = \lambda \Delta + 2\mu \epsilon_{zz} = -P(r,t) \tag{6}$$

where

$$\epsilon_{zz} = \frac{\partial S_z}{\partial z} ,$$

and that no tangential stress exists at the surface. (Kolsky: 195: 55)

$$\sigma_{rz}\Big|_{z=0} = 0 = \mu \left(\frac{\partial S_r}{\partial z} + \frac{\partial S_z}{\partial r} \right) . \tag{7}$$

Finite Difference Equations

The technique of finite differencing was chosen to solve the equations of motion primarily due to the ease and speed with which the equations could be implemented and solved on a digital computer. The equations were evaluated at the time-space mesh point i,j,n, where the finite difference mesh is described in Figure 5 and

$$S_r(r_i, z_j, t_n) = S_r(i\Delta r,\ j\Delta z,\ n\Delta t) = S_{r_{ijn}} .$$

A straight-forward application of central differences yields for S_r,

$$\left.\frac{\partial^2 S_r}{\partial t^2}\right|_{i,j,n} =$$

$$\frac{1}{\rho_{i,j,n}} \left\{ \frac{\partial}{\partial r} \left[\left(\frac{\partial S_r}{\partial r} + \frac{\partial S_z}{\partial z} \right) + 2\mu \frac{\partial S_r}{\partial r} + (\lambda + 2\mu) \frac{S_r}{r} \right]_{i,j,n} + \mu_{i,j,n} \frac{\partial}{\partial z} \left(\frac{\partial S_r}{\partial z} + \frac{\partial S_z}{\partial r} \right)_{i,j,n} \right\}$$

Or,

$$\frac{S_{r_{i,j,n+1}} - 2S_{r_{i,j,n}} + S_{r_{i,j,n-1}}}{\Delta t^2}$$

$$= \frac{1}{\rho_{i,j}} \left\{ \frac{\lambda_{i+\frac{1}{2},j} \left(\frac{\partial S_r}{\partial r} + \frac{\partial S_z}{\partial z} \right)_{i+\frac{1}{2},j,n}}{\Delta r} - \frac{\lambda_{i-\frac{1}{2},j} \left(\frac{\partial S_r}{\partial r} + \frac{\partial S_z}{\partial z} \right)_{i-\frac{1}{2},j,n}}{\Delta r} \right.$$

$$+ \quad \frac{2\mu_{i+\frac{1}{2},j}\left(\frac{\partial S_r}{\partial r}\right)_{i+\frac{1}{2},j,n} - 2\mu_{i-\frac{1}{2},j}\left(\frac{\partial S_r}{\partial r}\right)_{i-\frac{1}{2},j,n}}{\Delta r}$$

$$+ \quad \frac{(\lambda_{i+\frac{1}{2},j} + 2\mu_{i+\frac{1}{2},j})\left(\frac{S_r}{r}\right)_{i+\frac{1}{2},j,n}}{\Delta r}$$

$$- \quad \frac{(\lambda_{i-\frac{1}{2},j} + 2\mu_{i-\frac{1}{2},j})\left(\frac{S_r}{r}\right)_{i-\frac{1}{2},j,n}}{\Delta r}$$

$$+ \quad \mu_{i,j}\left[\frac{\left(\frac{\partial S_r}{\partial z} + \frac{\partial S_z}{\partial r}\right)_{i,j-\frac{1}{2},n} - \left(\frac{\partial S_r}{\partial z} + \frac{\partial S_z}{\partial r}\right)_{i,j+\frac{1}{2},n}}{\Delta z}\right]\Bigg\}. \qquad (8)$$

Because central differences were employed, the scheme will be accurate to second order in Δt, Δr, and Δz. The centering grid is given in Figure 6.

Similar implementation of the finite differencing for the S_z displacement and the boundary conditions causes Equations 3, 6, and 7 to become

$$\frac{S_{z_{i,j,n+1}} - 2S_{z_{i,j,n}} + S_{z_{i,j,n-1}}}{\Delta t^2} =$$

$$\frac{1}{\rho_{i,j}} \left\{ \frac{\lambda_{i,j-\frac{1}{2}} \left(\frac{\partial S_r}{\partial r} + \frac{\partial S_z}{\partial z} \right)_{i,j-\frac{1}{2},n}}{\Delta z} \right.$$

$$- \frac{\lambda_{i,j+\frac{1}{2}} \left(\frac{\partial S_r}{\partial r} + \frac{\partial S_z}{\partial z} \right)_{i,j+\frac{1}{2},n}}{\Delta z}$$

$$+ \frac{2\mu_{i,j-\frac{1}{2}} \left(\frac{\partial S_z}{\partial z} \right)_{i,j-\frac{1}{2}} - 2\mu_{i,j+\frac{1}{2}} \left(\frac{\partial S_z}{\partial z} \right)_{i,j+\frac{1}{2}}}{\Delta z}$$

$$+ \frac{(\lambda + 2\mu)_{i,j-\frac{1}{2}} \left(\frac{S_r}{r} \right)_{i,j-\frac{1}{2},n} - (\lambda + 2\mu)_{i,j+\frac{1}{2}} \left(\frac{S_r}{r} \right)_{i,j+\frac{1}{2},n}}{\Delta z}$$

$$+ \frac{\mu_{i+\frac{1}{2},j} \left(\frac{\partial S_r}{\partial z} + \frac{\partial S_z}{\partial r} \right)_{i+\frac{1}{2},j,n} - \mu_{i-\frac{1}{2},j} \left(\frac{\partial S_r}{\partial z} + \frac{\partial S_z}{\partial r} \right)_{i-\frac{1}{2},j,n}}{\Delta r}$$

$$\left. - \frac{\mu_{i,j}}{r_i} \left(\frac{\partial S_r}{\partial z} - \frac{\partial S_z}{\partial r} \right)_{i,j,n} \right\} \quad ; \qquad (9)$$

Figure 5. Definition of Finite Difference Mesh

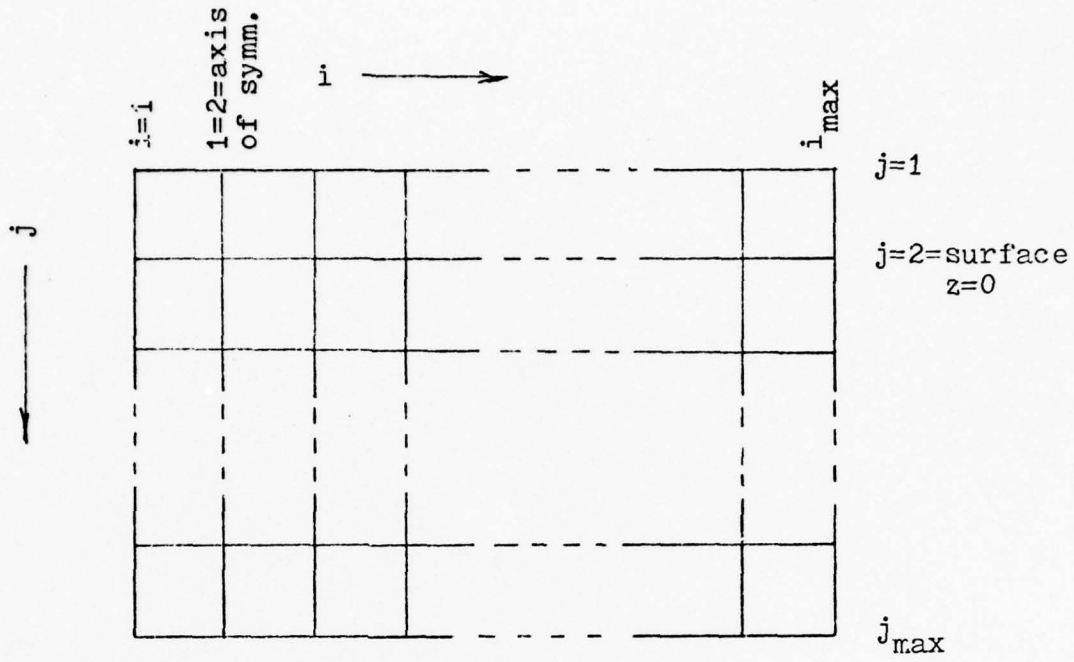

Figure 6. Centering Grid for the Finite Difference Equations

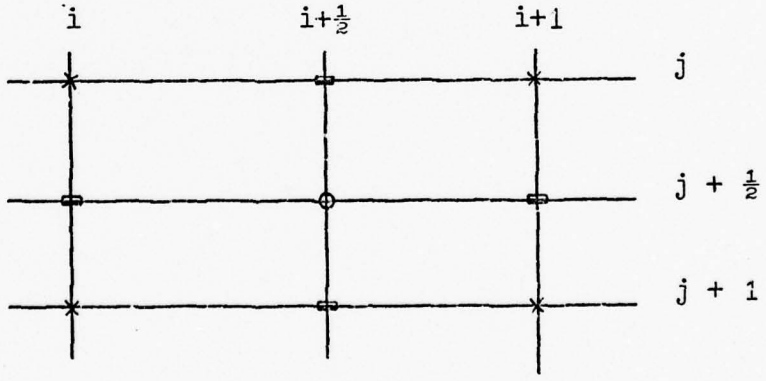

x are known values; ◻ are intermediate calculated values; o is the final calculated value

$$\left.\frac{\partial S_z}{\partial z}\right|_{z=0} = \frac{S_{z_{i,1,n}} - S_{z_{1,3,n}}}{2\,\Delta^z}$$

$$= -\frac{1}{(\lambda + 2\mu)_{i,2}} \left\{ \lambda_{i,2} \left(\frac{\partial S_r}{\partial r} + \frac{S_r}{r} \right)_{i,2,n} + P(r,t) \right\} \quad ; \qquad (10)$$

and

$$\left.\frac{\partial S_r}{\partial z}\right|_{z=0} = \frac{S_{r_{i,1,n}} - S_{r_{i,3,n}}}{2\,\Delta z}$$

$$= -\left.\frac{\partial S_z}{\partial r}\right|_{z=0} = \frac{S_{z_{i-1,2,n}} - S_{z_{i+1,2,n}}}{2\,\Delta^r} \quad . \qquad (11)$$

Because the displacement values at time n and n-1 will be zero until airshock arrival, the only unknowns in Equations 8-11 are the time advanced (n+1) values. Thus, the scheme as chosen is a second-order accurate, explicit algorithm.

Surface Pressure

Finally, before implementation on the computer the surface pressure input P(r,t) is required. Because scaled near-proximity of the bursts to the ground is necessary to achieve an airblast precursor, surface effects upon the overpressure have to be considered. The blast data curves in Glasstone's, The Effects of Nuclear Weapons were taken as reference data because of his inclusion of ground effects.

For the typical overpressure waveform shown in Figure 7, the following parameters are required: time of arrival TARR, peak overpressure PEAKP, duration of the positive overpressure phase TPLUS, and the rate of decay of pressure with time.

General algorithms were found for TARR and derived for the rate of decay of the pressure with time. The first is given as follows (Liner, 1975: 1972-3):

$$TARR = \frac{0.54291\ Y - 21.185\ r_s\ Y^{2/3} + 361.8\ r_s^2 Y^{1/3} + 2383\ r_s^2}{Y^{2/3} + 2.048\ r_s\ Y^{1/3} + 2.6872\ r_s^2}$$

where

TARR is in msec,

Y = weapon yield in kilotons, and

r_s = slant range in kilofeet.

For a surface burst

$$TARR\ (HOB = 0) = TARR\ (2Y, r_s).$$

Figure 7. Typical Overpressure Waveform (Glasstone, 1977: 84)

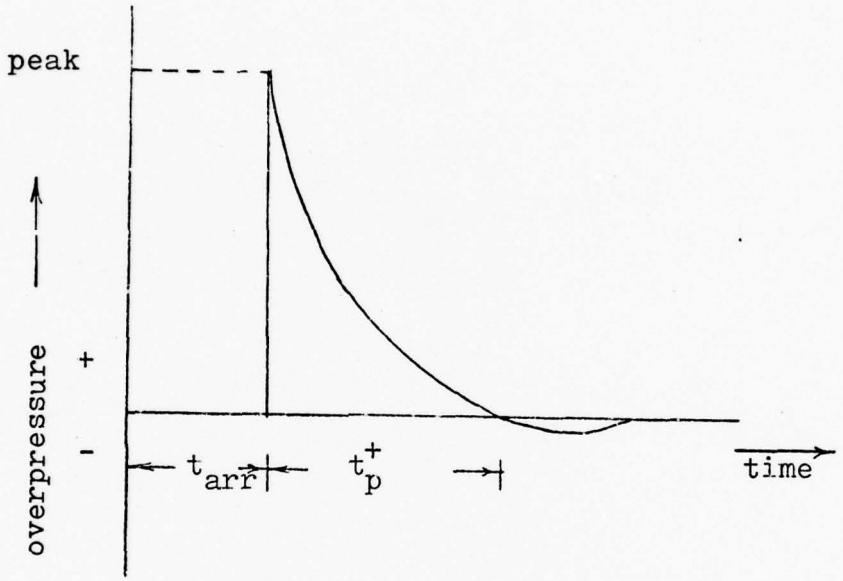

t_{arr} = arrival time of shock front

t_p^+ = duration of positive pressure phase

(negative pressure phase will be ignored in this model)

For a non-surface burst, the free air arrival time is used in the regular reflection region and a linear interpolation between free air and surface burst values is made in the Mach reflection region.

$$TARR = TARR(Y,r_s), \text{ for } \frac{HOB}{\text{ground range}} \geq 1;$$

$$= TARR(Y,r_s) * \frac{HOB}{\text{ground range}} +$$

$$TARR(2Y,r_s) * \left(1 - \frac{HOB}{\text{ground range}}\right), \text{ for } \frac{HOB}{\text{ground range}} \leq 1.$$

The second parameter, decay of overpressure with time, is given by

$$\frac{P(TAU)}{PEAKP} = 1 - \left[1 - (1 - TAU)^m\right]^{1/m}$$

where

$$TAU = \frac{t - TARR}{TPLUS}, \quad \text{and}$$

$$m = 1 + .382\,(\ln PEAKP) - .136\,(\ln PEAKP)^2 + .025\,(\ln PEAKP)^3 .$$

The computational algorithm for TARR was originally derived by Brode and that for P(t) was derived by applying curvefitting techniques (Appendix C) to the Glasstone data for overpressure decay. (Glasstone, 1977: 100)

At the time of computer implementation no suitable, general algorithms had been found for PEAKP and TPLUS. The

technique chosen, then, was to fit the Glasstone data for these parameters by linear segmentation for each specific problem simulated. This aspect, while speeding initial implementation, adds significant awkardness when applying the code to various burst problems. A minor improvement was achieved by calculating the pressure as a function subprogram. For differing events the unique overpressure function can be validated independently and then appended to the main program. (Glasstone, 1977: 111-115, 119)

Treatment of Boundary Displacements

The two stress components on the surface (the normal stress defined by the overpressure and the identically zero tangential stress) provide the calculational means to derive the displacements at the top boundary of the finite difference mesh. These were given analytically by Equations 6 and 7 and in finite difference form by Equations 10 and 11.

Symmetry is the key by which the displacements at the lefthand mesh boundary are found. Because ground zero is the symmetry axis, displacements immediately to either side are considered equal. By averaging these mirrored displacements, the displacements at the lefthand mesh boundary or ground zero are found and are equal to those just averaged.

Finally, the righthand and bottom mesh displacements must be defined. The simplest choice is to apply rigid boundaries; that is, the displacements there remain zero. One particularly annoying property of such a treatment is that reflection of seismic signals occurs at these rigid boundaries.

This trait becomes particularly restrictive when attempting to compare model output data to published late-time seismic motions from test data and independent elastic calculations.

Interference of reflected signals can be prevented. Two computationally easy choices can readily be implemented: increase the mesh size or stop the computation before any reflected signal can reach the point of interest.

Increasing the mesh size can be done by increasing the spatial mesh increments, thereby losing accuracy, or by increasing the computer memory requirements of the calculation. Stopping the computation before reflection can affect the motion of the point of interest can, as in late-time motion, result in shutdown before significant motion has occurred at the point of interest.

Another choice which is more difficult computationally is to develop a transmitting boundary; that is, a boundary which acts as nearly as possible as though a semi-infinite region of material exists beyond the mesh boundary. If successfully accomplished, a seismic signal can be transmitted across the boundary with no reflection; and, the mesh could be kept resonably compact, yet still yield acceptably accurate results.

The nature of the airblast-induced precursor requires that surface seismic motions be computed over a ground range which is long in comparison to the ground depth of interest. As a result a relatively shallow mesh grid is used. Because reflections from the bottom of the mesh would therefore occur

first, the bottom mesh boundary was chosen for the application of the transmitting boundary.

The requirement upon such a boundary is that it must act as a one-way valve. This one-way action can be accomplished by permitting a seismic disturbance incident upon the boundary from above to pass out of the mesh and disappear into the imaginary half-space below while simultaneously preventing the return of reflected signals into the mesh.

The means by which this action will be performed is based upon a momentum flux argument. Consider the mesh as it exists in Figure 8 near the bottom boundary. At the points marked with the symbol X, the displacements S_r and S_z are known. From these displacements, calculations of velocities, spatial derivatives, and stress components can be made for the point P centered at $i+\frac{1}{2}$ and JMAX-3/2.

The stress component σ_{zz} represents the flux of z-momentum in the z-direction, and component σ_{rz}, the flux of r-momentum in the z-direction. A properly constructed transmitting boundary permits the net outward flow of momentum. However, it prevents the net inward flow of momentum because this results in the undesirable increase of momentum within the finite difference computational grid.

Therefore, if the proper flow of momentum is indicated at point P (Appendix D presents the derivation of the logic table and equations for the transmitting boundary), this momentum is allowed to flow across the boundary (level JMAX-1) by equating the stress at point P to that at point R centered across the

Figure 8. Finite Difference Mesh Grid Near Bottom Boundary

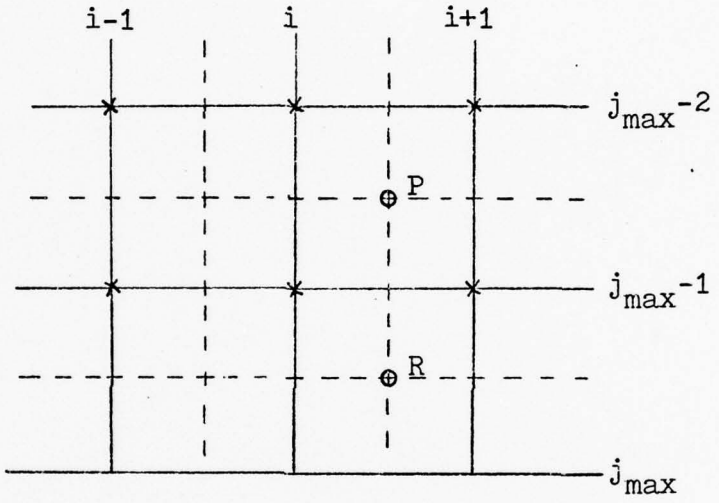

boundary at $i+\frac{1}{2}$ and $JMAX-\frac{1}{2}$. If the conditions indicate improper flow of momentum, the stress components at R are set to zero. Next, displacements along level j=JMAX are calculated from the centering scheme, where the displacements at the lower right-hand corner of the mesh are zero and the computational march is executed along the j=JMAX level from i=IMAX-1 to i=3.

Of course, a trade-off does exist when using such a transmitting boundary. This is that momentum transferred out of the mesh is lost and can play no part in the elastic rebound of the medium. For airblast-induced seismic motions this limitation is expected to occur far too late to be of concern.

Method of Solution

The explicit, second-order finite difference scheme derived earlier involves two known time levels (n-1 and n) and three known spatial levels in both the radial (i-1, i, i+1) and vertical (j+1, j, j-1) directions. The task is then to calculate the unknown, time-advanced (n+1) values for all the spatial mesh points of interest. Figure 9 presents as a flow chart the method by which the computational model solves the equations of motion.

Data characterizing the burst, ground medium, finite difference mesh parameters, and output options are first input. An array describing the ground properties within the mesh is constructed. Next, the overpressures on the ground surface are calculated and used by the boundary condition equations. These equations give the displacements at the uppermost boundary of the finite difference mesh, and the symmetry condition is used to find the displacements at the leftmost boundary. Utilizing the main difference equations for the seismic displacements and marching through the spatial mesh, the displacements are found for each mesh point except at the righthand and bottom boundaries.

No displacements are calculated at the righthand boundary because a rigid boundary condition is used. For the bottom, either a rigid boundary condition or a transmitting boundary condition based on a momentum transfer argument is applied (Appendix D). All of the desired time-advanced displacements throughout the mesh have not been calculated.

Figure 9. Method of Solution

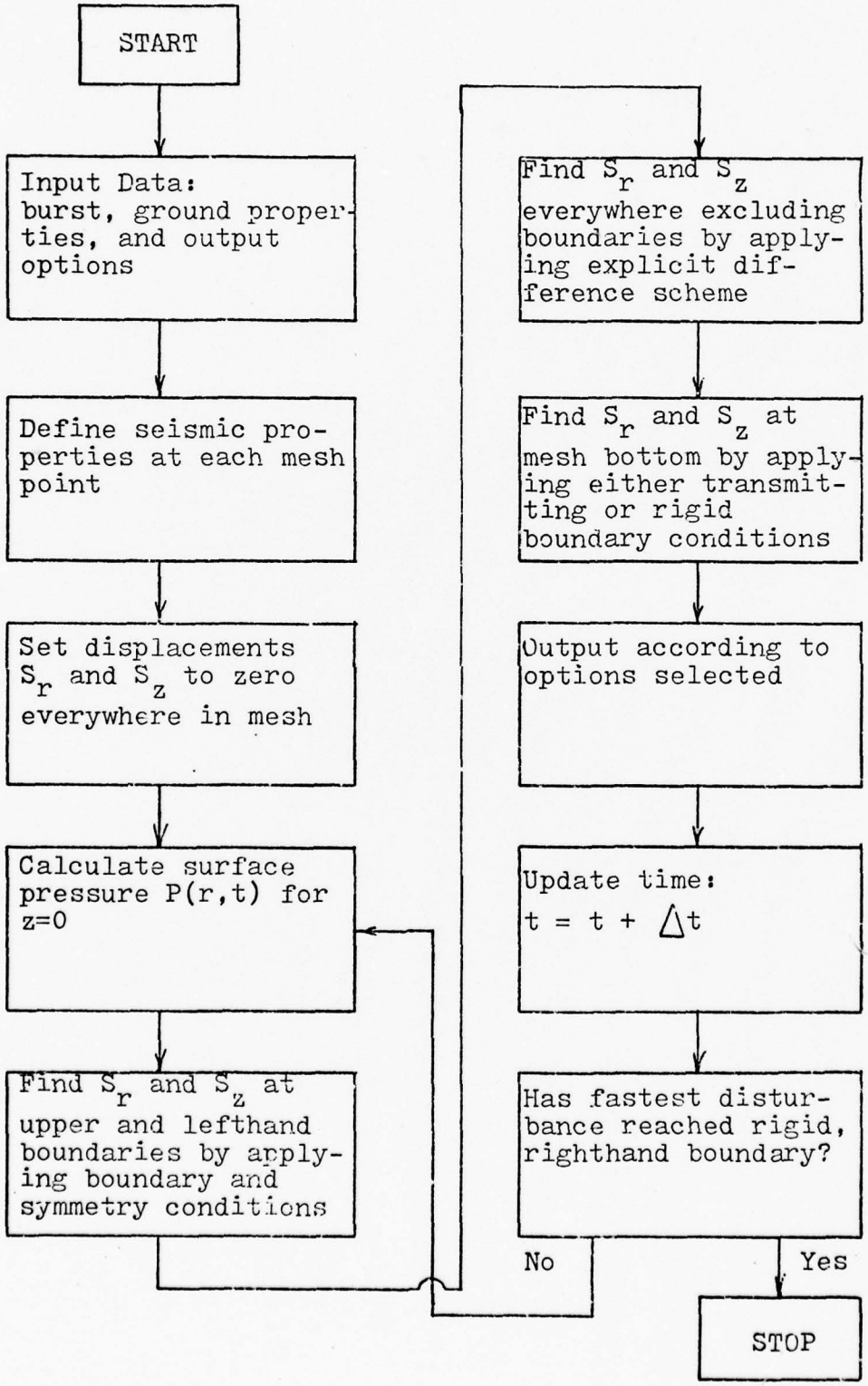

Finally, the output format chosen by the input options is executed, and the process is repeated, beginning with an advanced time and updated surface pressure.

This iterative process continues until the desired shutdown time is reached. Typically, this shutdown time is chosen as the time of first arrival of seismic waves at the righthand rigid boundary. Thus, unwanted, artificial reflections are prevented.

III. Code Calculations

Stability

One of the prime questions arising when using any finite difference scheme is whether the scheme is stable. The artificial, non-physical inaccuracies introduced by the presence of instability are governed by the choice of time step Δt and grid element sizes Δr and Δz.

Two different stability criteria were initially speculated to be applicable to this model. The first, St_1, was set forth by the Army Corps of Engineers investigators as applicable to two-dimensional finite difference calculations of ground shock which outruns the airblast. This condition was presented as the Courant, Fredricks, and Levy stability requirement, namely, (Hadala, 1973: 42)

$$\Delta t \leq \frac{\Delta x}{\sqrt{2}\ V_{max}} \qquad \text{(sec)},$$

where Δt = time step,

Δx = spatial mesh increment = $\Delta r = \Delta z$, and

V_{max} = maximum disturbance propagation velocity.

The second stability criterion, St_2, was based on the physical argument that no disburbance should be allowed to propagate a distance greater than the mesh spacing Δr or Δz in one time step Δt. Mathematically, this is given as

$$\Delta t \leq \frac{\Delta x}{V_{max}} \qquad \text{(sec)} \quad .$$

In order to determine which of the two preceding stability conditions in fact apply to this model, an experimental stability analysis was conducted. Figures 10-12 present the results of this stability analysis. This analysis consisted of making several runs with the computer model to calculate a ground shock problem. All runs are the same except that the time step has been changed in each run. The time step for each run is shown in relation to both stability criteria, St_1 and St_2. While some far-field oscillations appear for $\Delta t = .002$ sec (which exceeds the stability criterion St_1 set forth by Hadala), the solution has not become unstable. Instead, this indicates that the stability condition is being approached. Further enlargements of the time step show that the less restrictive, physically-derived condition, St_2, should be applied as the stability limitation to the difference scheme of this model.

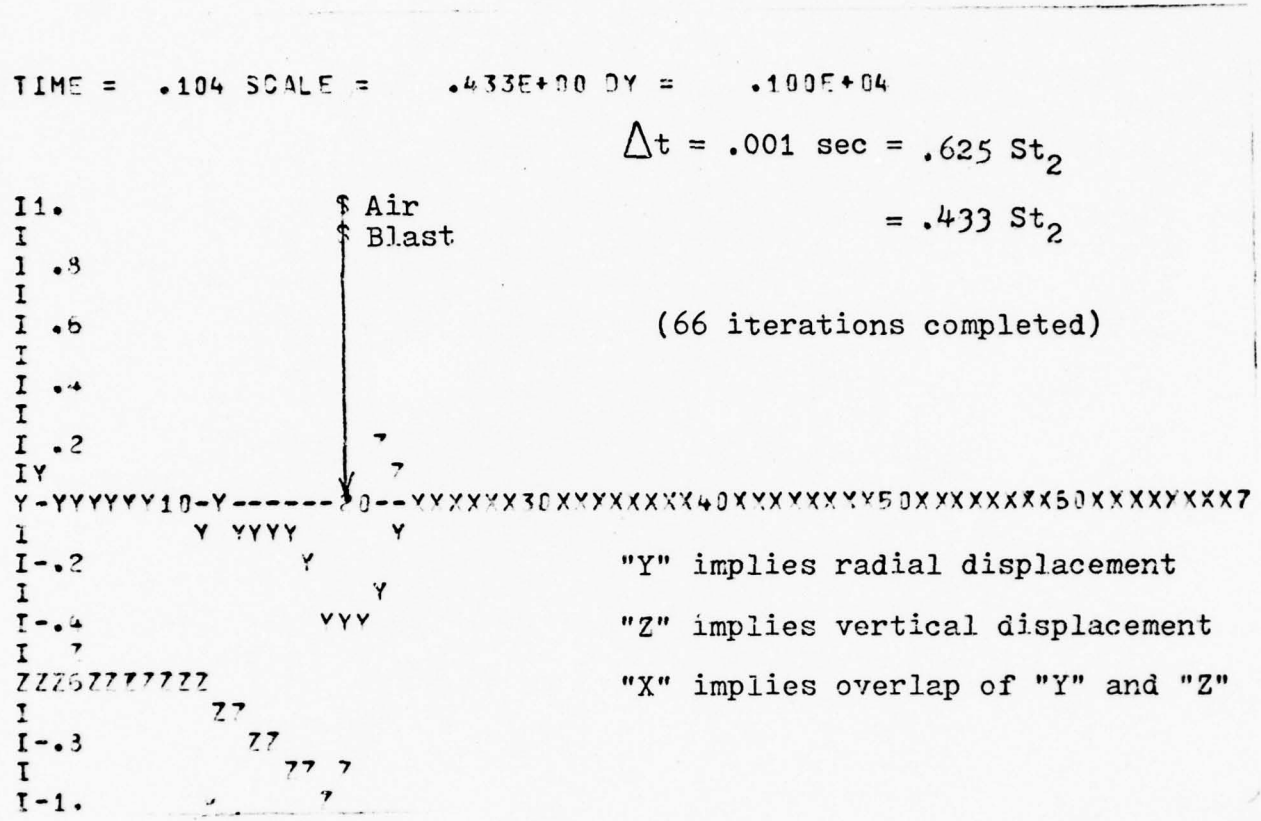

Figure 10. Stability Analysis, 1 Msec Time Step

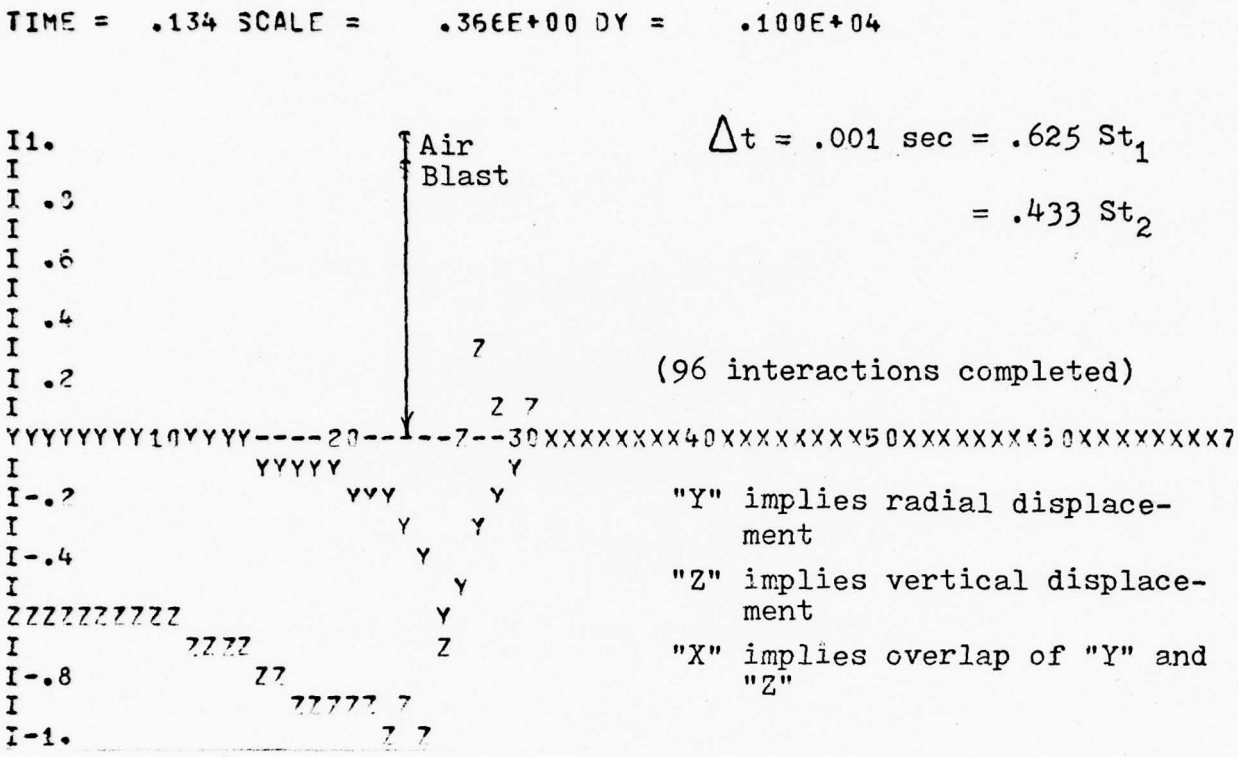

Figure 10. Cont. . .

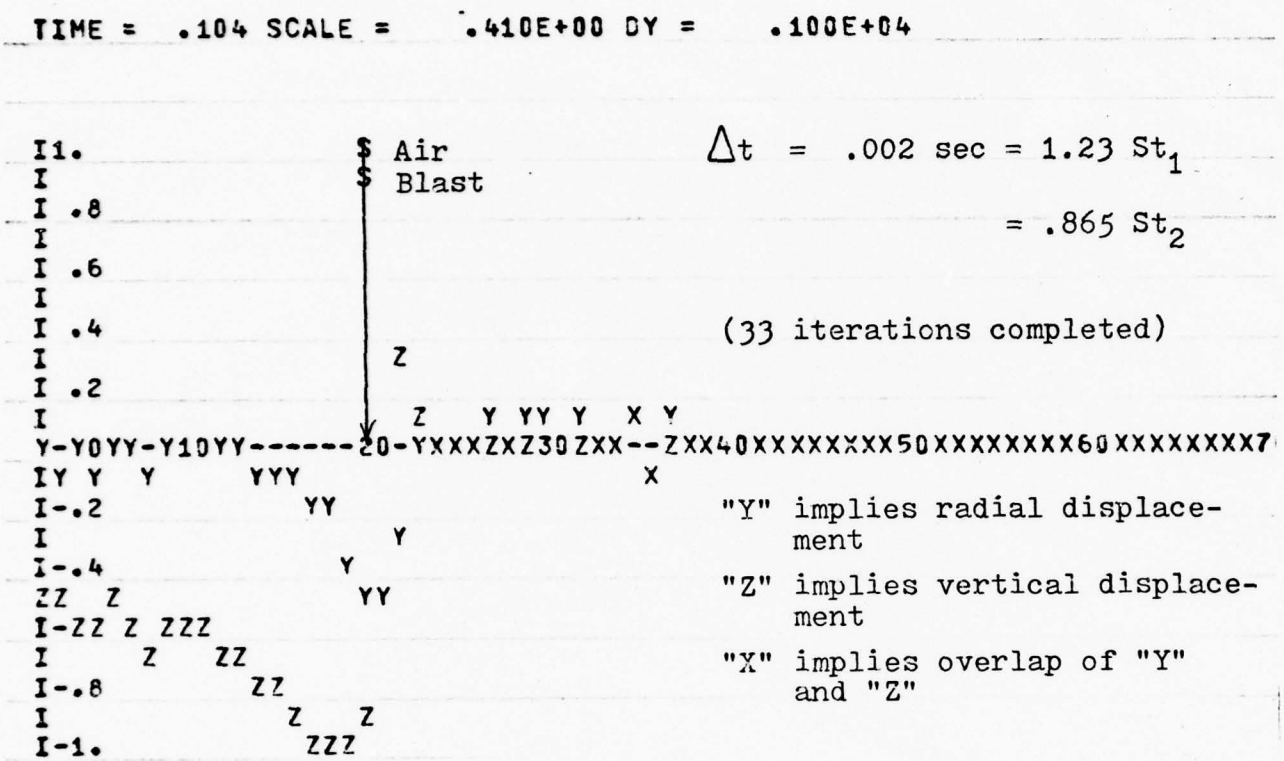

Figure 11. Stability Analysis, 2 Msec Time Step

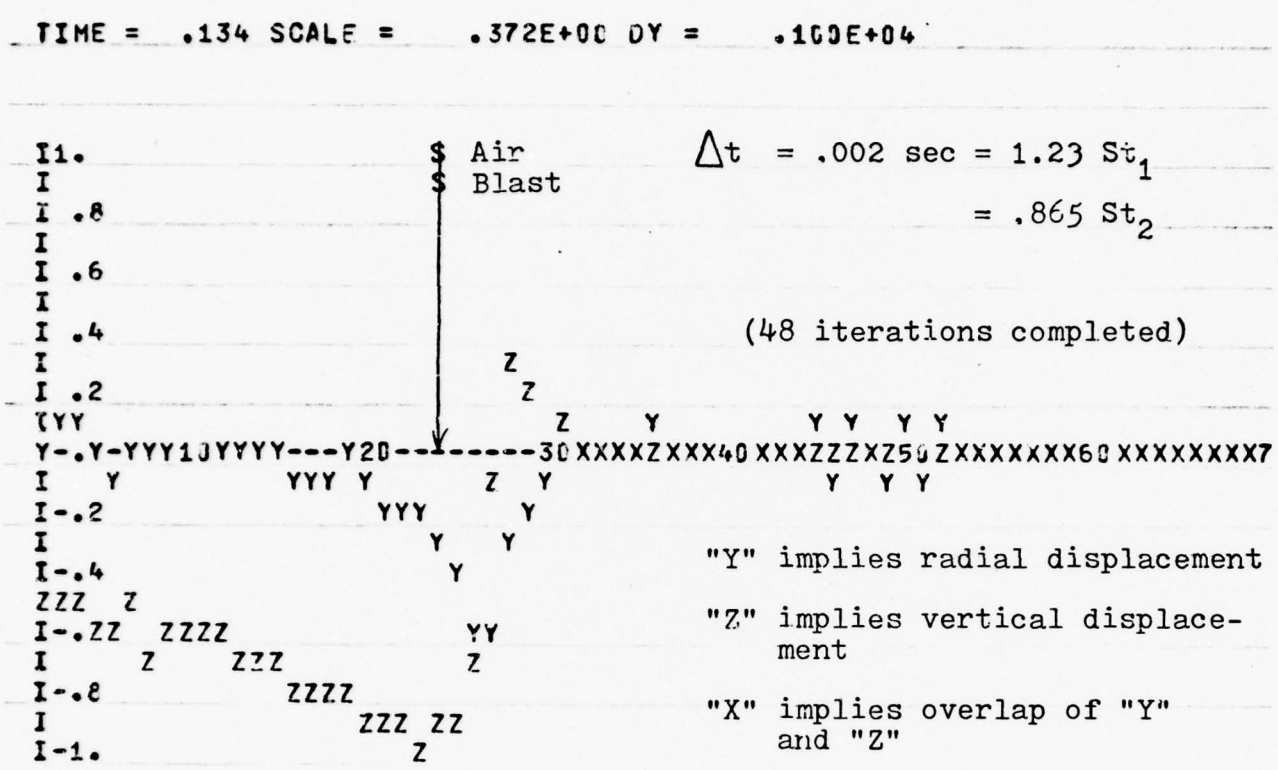

Figure 11. Cont. . .

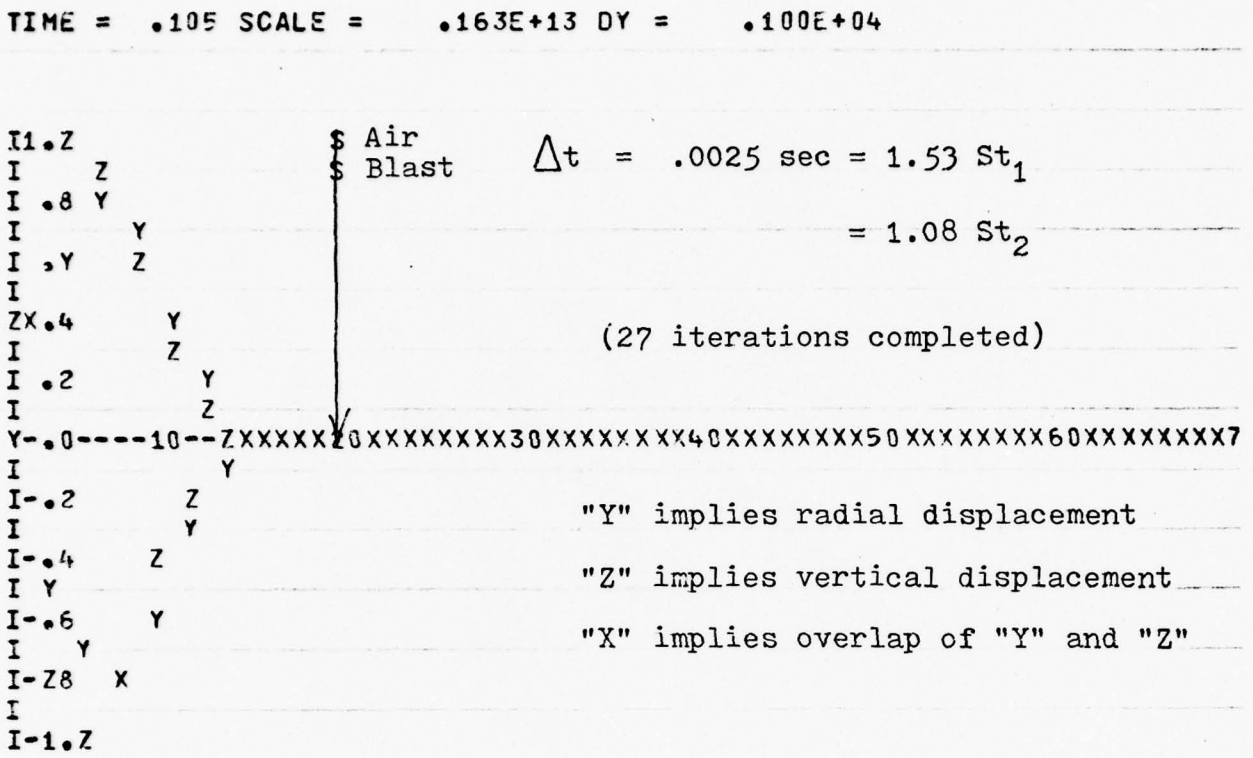

Figure 12. Stability Analysis, 2.5 Msec Time Step

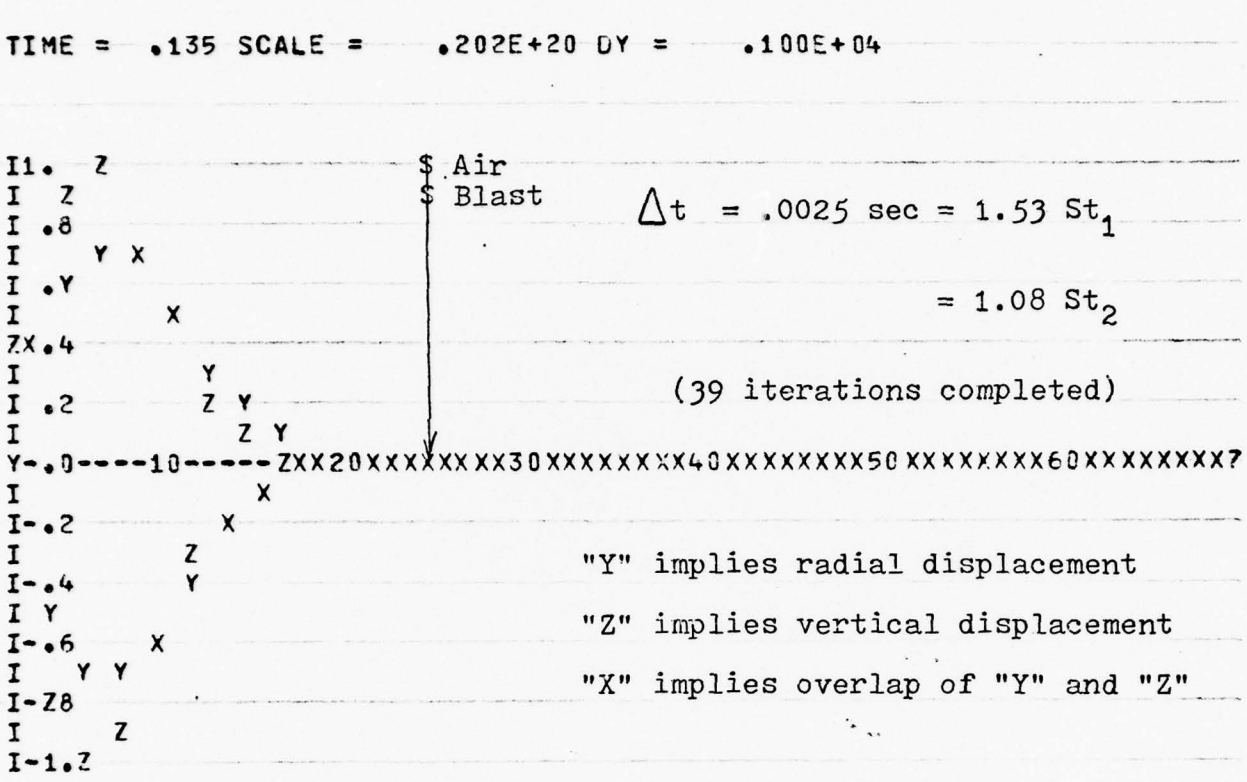

Figure 12. Cont. . .

Transmitting Boundary

Figures 13-16 present a comparison of surface seismic motions computed by the computer model. Three different but related problems are represented. One is a "standard" employing a rigid bottom boundary and 100 by 25 mesh grid for comparison with the results obtained using a transmitting boundary. The second differs from the "standard" only by using a transmitting bottom boundary. Lastly, the third employs a transmitting bottom boundary and a reduced 100 by 10 mesh grid. However, the mesh spacing in the third run is the same as in the standard. The purpose of this third run is to test whether the transmitting boundary as constructed would permit the execution of a problem with a reduced number of mesh points while faithfully reproducing the results obtained with a larger number of grid points.

The first and second runs are identical (Figures 13 and 14) until just after t = .4161 when the close-in waveform and magnitudes change slightly. These changes reasonably coincide with the earliest possible arrival at the surface (t = .4166) of a bottom reflected signal in Run #1. As would be expected the surface displacements after t = .4266 are more negative in Run #2 in which reflection has been prevented. Table II shows the surface vertical displacements for mesh point (i = 13, j = 2) from Run #1 (standard, rigid bottom boundary) in comparison with Run #2 (transmitting boundary) in which reflection has been prevented.

But, unlike the encouraging results obtained with Run #2, Run #3 deviates from the "standard" at an earlier time than is expected from computing the earliest possible arrival time of a bottom-reflected signal, with the surface displacements becoming significantly larger. This result casts a shadow of uncertainty over the validity of the transmitting boundary being utilized.

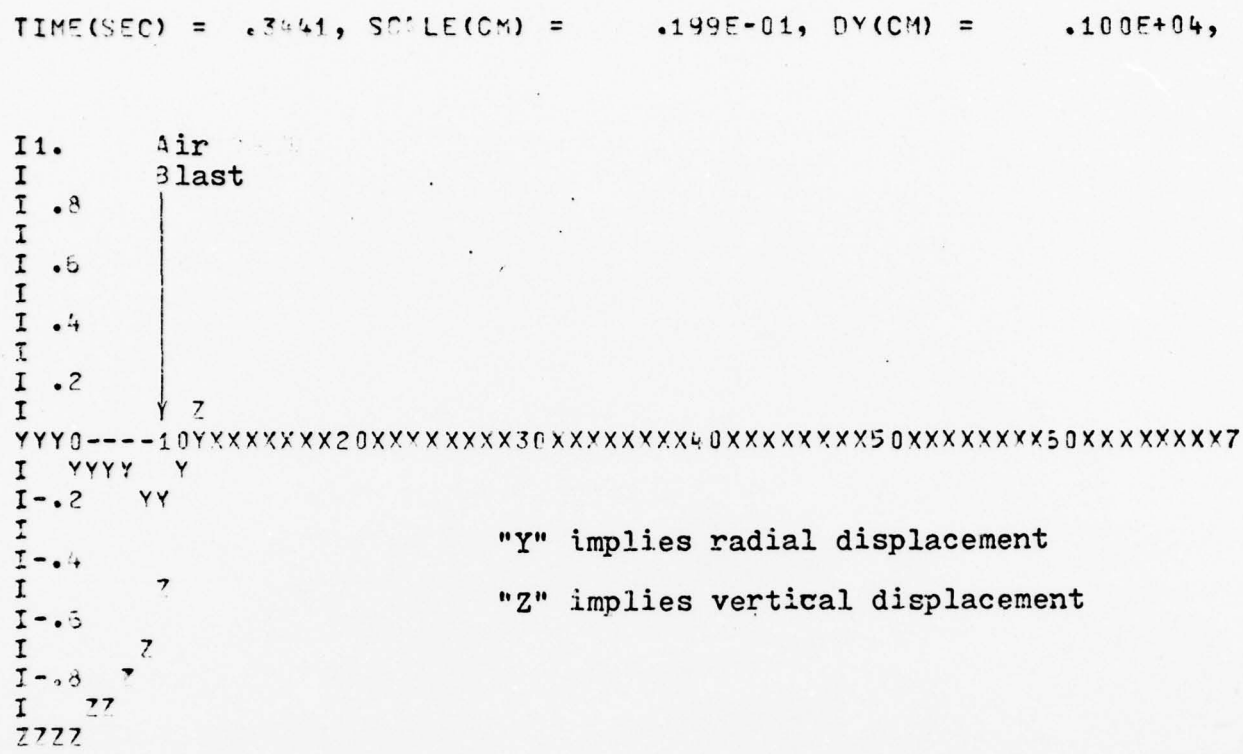

Figure 13. Computations with Model to Test Operation of the Transmitting Boundary - "Standard" with Rigid Bottom Boundary

```
TIME(SEC) =  .4151, SCALE(CM) =     .228E-01, DY(CM) =     .100E+04,


I1.              Air
I                Blast
I .8
I
I .6
I
I .4
I
I .2
I                                  ZZ
YYYYYY--10---------20---7--XX30XXXXXXXX40XXXXXXXX50XXXXXXXX60XXXXXXXX7(
I      YYYYYY                      YY
I-.2          YYYYYYYYYXXXY
I                      7
I-.4                 ZZ
I
I-.6                Z
I
I-.8
ZZZZZ ZZ        ZZ
I-1. Z  ZZZZZZ
```

Figure 13. cont . . .

TIME(SEC) = .4341, SCALE(CM) = .2125-01, DY(CM) = .100E+04,

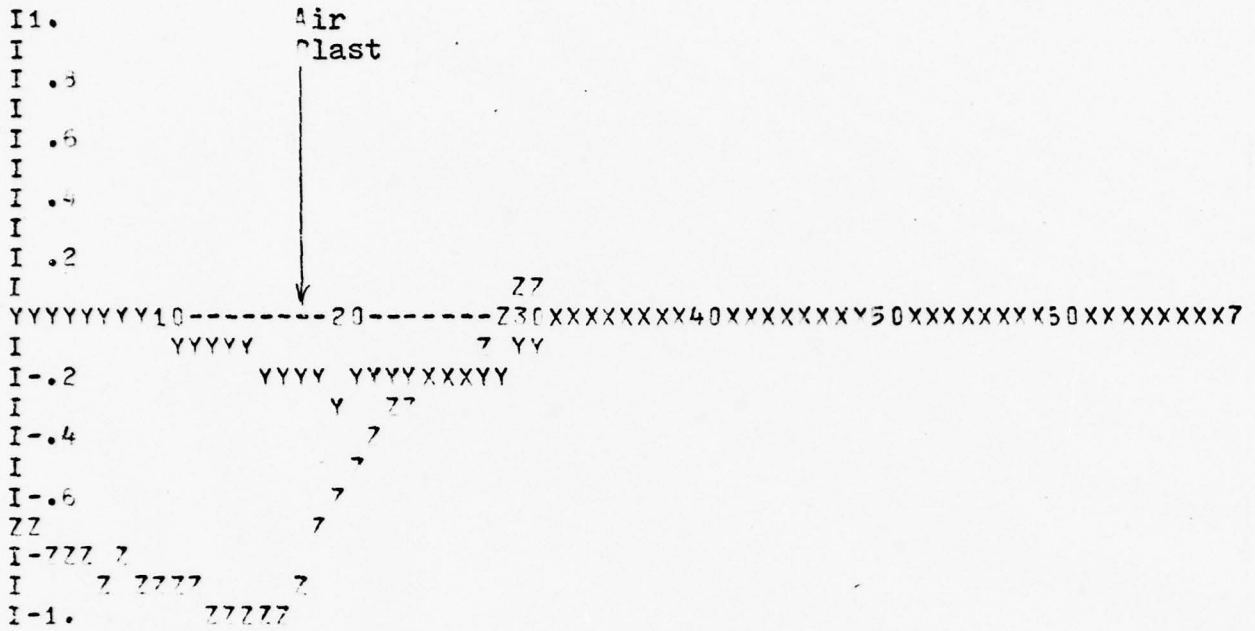

Figure 13. cont...

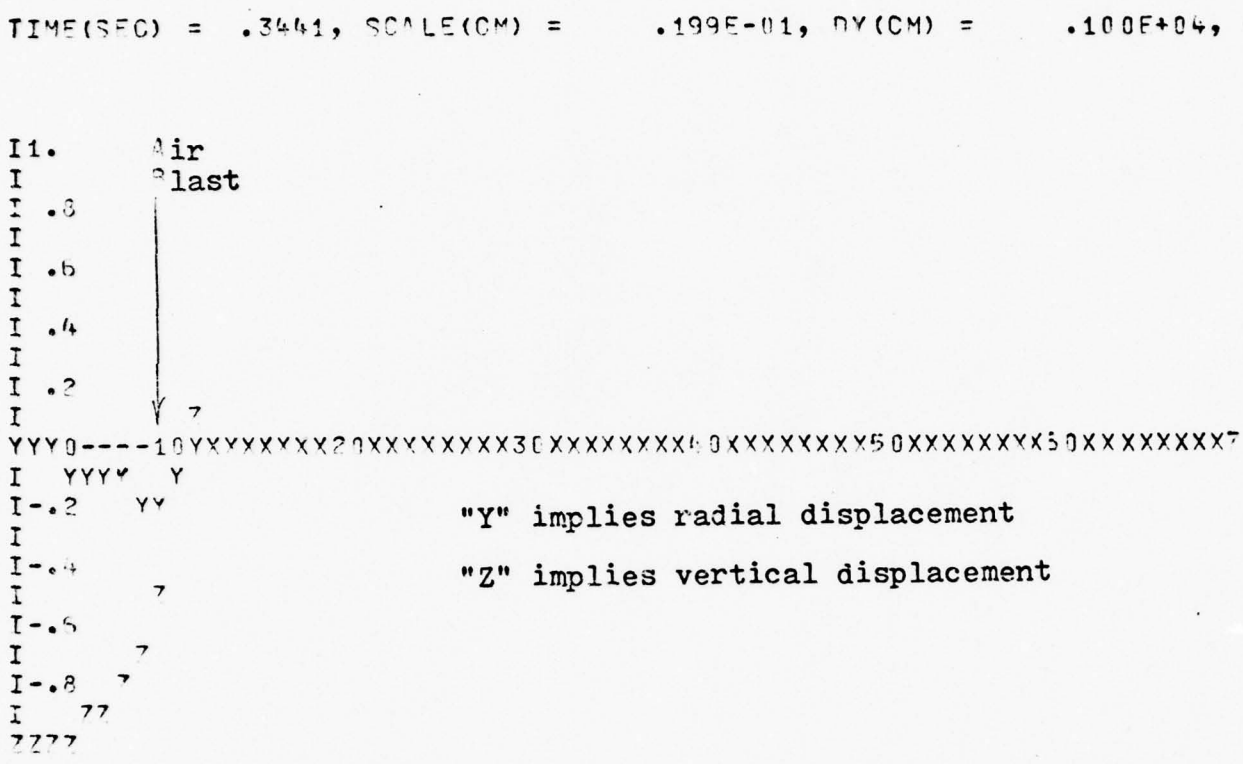

Figure 14. Computations with Model to Test Operation of the Transmitting Boundary - 100x25 Mesh with Bottom Transmitting Boundary

TIME(SEC) = .4151, SCALE(CM) = .229E-01, DY(CM) = .100E+04,

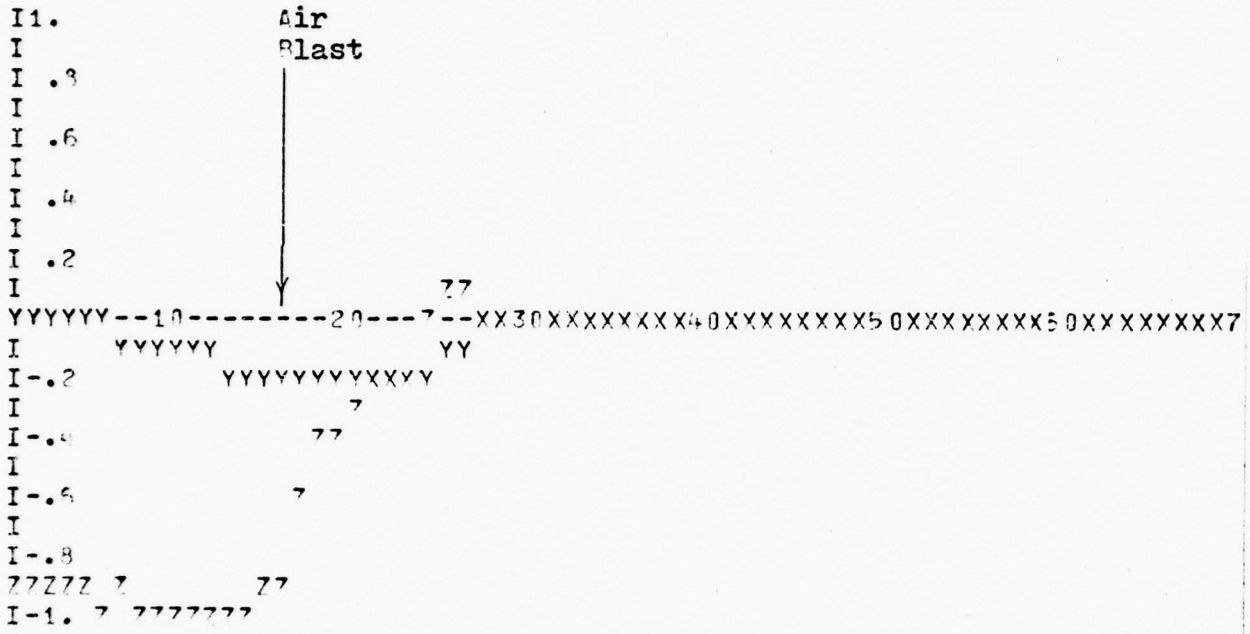

Figure 14. cont . . .

```
TIME(SEC) =  .4341, SCALE(CM) =      .243E-01, DY(CM) =      .100E+04,

I1.                Air
I                  Blast
I .8                |
I                   |
I .6                |
I                   |
I .4                |
I                   |
I .2                |
I                   V              77
YYYYY---10--------20-------730XXXXXXXX+0XXXXXXXXX50XXXXXXXX50XXXXXXXXX7
I     YYYYYYY                    7 YY
I-.2          YYYYYY  YYYYYXXXYY
I                     Y   77
I-.4                    7
I                      7
I-.6                  7
I                    7
77.8
I 7777777          7
I-1.     77777777
```

Figure 14. cont . . .

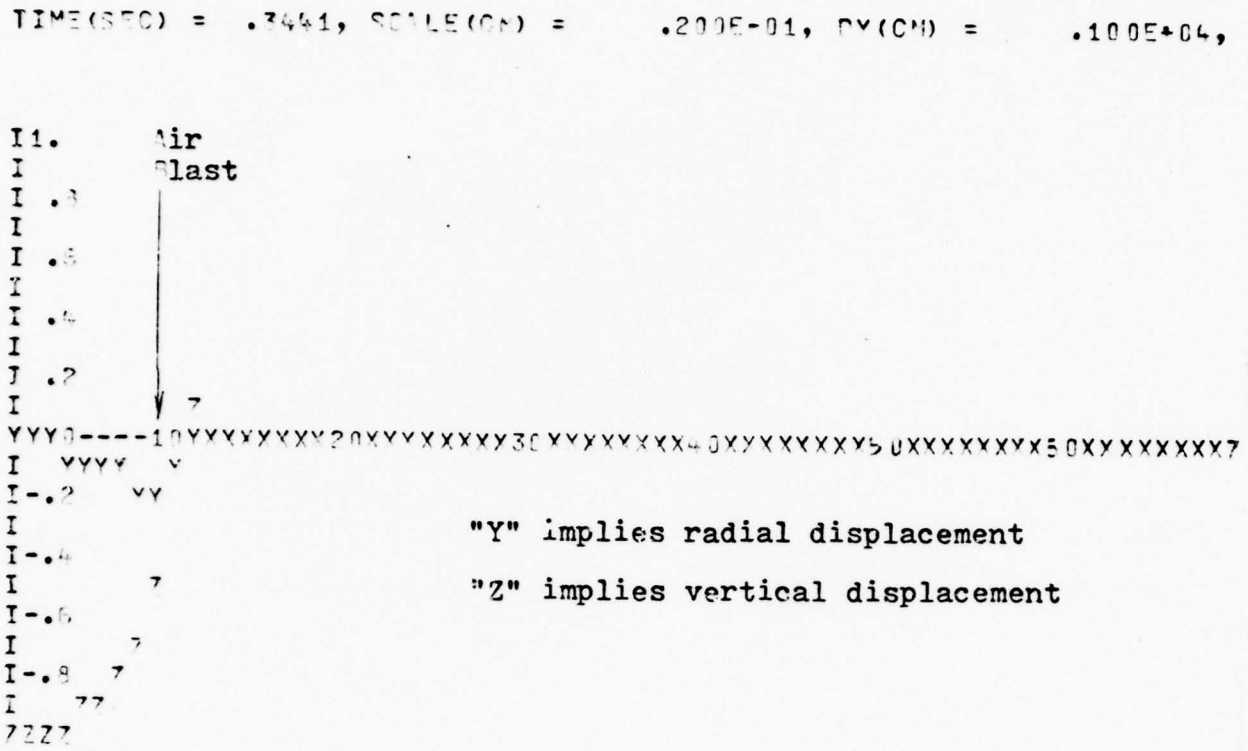

Figure 15. Computations with Model to Test Operation of the Transmitting Boundary - 100x10 Mesh with Bottom Transmitting Boundary

```
TIME(SEC) =  .4151, SCALE(CM) =      .102E+00, DY(CM) =      .100E+04,

I1.              Air
I                Blast
I  .8
I
I  .6
I
I  .4
I
I  .2
I
YYY0----10--------20777XXXX30XXXXXXXX40XXXXXXXX50XXXXXXXX60XXXXXXXX7
I   YYYY            7YYYYYY
I-.2    YYYYYYYYYYY
I                  7
I-.4             77
I              77
I-.6      777
I        7
I-.87 7
I   7 7
ZZZ.
```

Figure 15. cont . . .

```
TIME(SEC) =  .4341, SCALE(CM) =      .113E+00, DY(CM) =      .100E+04,

I1.                Air
I                  Blast
I .8
I
I .6
I
I .4
I
I YYY
I
YY.0-Y--10--------20--ZZZZZX30XXXXXXXX40XXXXXXXX50XXXXXXXX60XXXXXXX7
I                    ZZYYYYYY
I-.2  YY      YYYYYYYY
I        YYYYY    Z
I-.4              ZZ
I Z            ZZ
I-.6         Z
ZZ      ZZ Z
I-.Z  Z  Z
I
I-1.ZZ
```

Figure 15. cont . . .

Table II. Comparison of Surface Seismic Motions - Rigid Versus Transmitting Bottom Boundaries

Surface Vertical Displacements
at Mesh Point (i=13, j=1)

Time (sec)	Standard w/rigid Boundary (cm)	100x25 Mesh with Transmit. Boundary (cm)	100x10 Mesh with Transmit. Boundary (cm)
0.311	0.0	0.0	0.0
0.350	0.021	0.021	0.022
0.375	-0.017	-0.017	-0.015
0.400	-0.023	-0.023	-0.040
0.425	-0.023	-0.023	-0.050
0.450	-0.018	-0.025	-0.060
0.475	-0.009	-0.030	-0.061
0.500	-0.003	-0.004	-0.012

Simulation of a 28 Kiloton Atmospheric Burst

With the preceding analysis completed, the model is next used to simulate the airblast-induced ground motions from an atmospheric burst. A yield of 28 kilotons is chosen, with detonation occurring at a height of burst of 165 feet. This height of burst is intermediate to those for events in Table I detonated at Frenchman Flats and displaying an airshock precursor. Appendix F gives the subroutine which calculates the airblast parameters on the ground for this event.

The seismic reactions of four different ground media are compiled in the tables which follow. This compilation results from the use of the computer model with rigid right-hand and bottom boundaries. From run to run, only the ground medium over which the burst is assumed to occur is changed. These four ground media are described in Figure 16.

The resulting maximum upward surface velocities are given in Tables III-V. These velocities were obtained by differentiation of the vertical surface displacements computed with the model. No maximum velocities are given for Run #4 which simulated the Frenchman Flats test site because all upward velocities were less than 0.1 cm/sec and considered insignificant. Failure of this layered medium to produce the enhanced velocities indicated as possible in Appendix B is apparently due to the presence of the very slow upper layer where the seismic velocity is only slightly greater than the sound speed in ambient air.

Figure 16. Ground Media for Model Simulation of 28 Kiloton Event

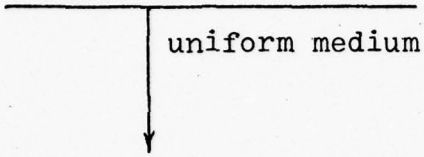

Run #1

v_p = 1.22 km/sec

λ = 1.14E10 dynes/cm^2

μ = 1.14E10 dynes/cm^2

ρ = 1.9 gm/cm^3

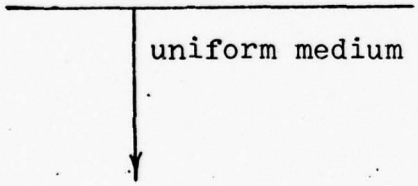

Run #2

v_p = 1.82 km/sec

λ = 3.70E10 dynes/cm^2

μ = 1.49E10 dynes/cm^2

ρ = 2.0 gm/cm^3

Figure 16. Cont. . . .

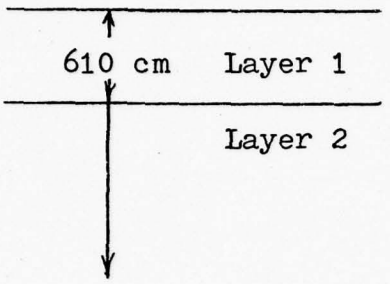

Run #3

v_{p_1} = 0.35 km/sec

ρ_1 = 1.7 gm/cm^3

λ_1 = 1.16E9 dynes/cm^2

μ_1 = 4.68E8 dynes/cm^2

v_{p_2} = 1.82 km/sec

ρ_2 = 2.0 gm/cm^3

λ_2 = 3.70E10 dynes/cm^2

μ_2 = 1.49E10 dynes/cm^2

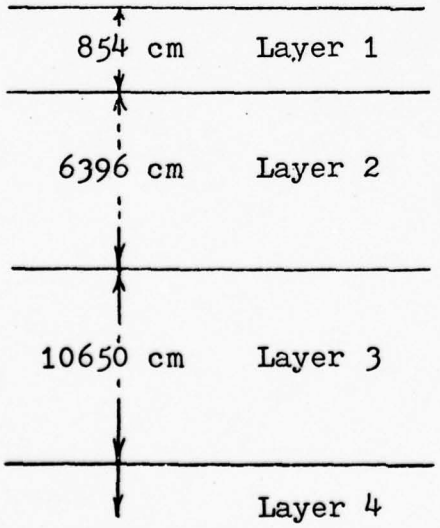

Run #4

Simulates Frenchman Flats (Hadala, 1973: 145, 281)

v_{p_1} = 0.35 km/sec

v_{p_2} = 0.76 km/sec

v_{p_3} = 1.82 km/sec

v_{p_4} = 2.45 km/sec

Mesh point i	6	7	8	9	10	11	12	13	14	15	16
Maximum upward surface velocity (cm/sec)	0	0	0	1.3	0.9	1.9	2.2	3.5	5.8	6.7	12.3
T1, time of max velocity (sec)	--	--	--	.0455	.0515	.0515	.0545	.0605	.0635	.0695	.0755
T2, time of airblast arrival (sec)	.0407	.0425	.0447	.0473	.0503	.0537	.0575	.0618	.0665	.0716	.0772
% of fireball energy emitted prior to T1	--	--	--	< 1	< 1	~ 1	~ 1	< 2	< 2	~ 2	~ 3
% of fireball energy emitted in (T2-T1) sec.	--	--	--	< 1	< 1	< 1	< 1	< 1	< 1	< 1	< 1

Mesh point i	17	18	19	20	21	22	23	24	25	26	27
Maximum upward surface velocity (cm/sec)	11.0	13.0	11.3	13.7	13.0	11.7	10.7	12.0	10.0	10.0	9.0
T1, time of max velocity (sec)	.0815	.0875	.0935	.0995	.1055	.1115	.1175	.1235	.1325	.1385	.1475
T2, time of airblast arrival (sec)	.0832	.0885	.0939	.0997	.1059	.1125	.1195	.1268	.1346	.1427	.1511
% of fireball energy emitted prior to T1	~ 3	~ 3	~ 4	~ 5	~ 5	~ 5	~ 6	~ 7	~ 9	~ 9	~ 11
% of fireball energy emitted in (T2-T1) sec	< 1	< 1	< 1	< 1	< 1	< 1	< 1	~ 1	< 1	< 1	~ 1

Table III. Surface Velocity Data in Varied Ground Media - Run #1

Mesh point i	28	29	30	31	32	33					
Maximum upward surface velocity (cm/sec)	9.0	8.3	7.7	7.0	5.7	4.7					
T1, time of max velocity (sec)	.1565	.1625	.1715	.1805	.1895	.1985					
T2, time of airblast arrival (sec)	.1599	.1691	.1786	.1884	.1986	.2091					
% of fireball energy emitted prior to T1	~ 15	~ 17	~ 18	~ 20	~ 21	~ 22					
% of fireball energy emitted in (T2-T1) sec.	~ 2	~ 1	~ 1	~ 2	~ 2	~ 5					
Mesh point i											
Maximum upward surface velocity (cm/sec)											
T1, time of max velocity (sec)											
T2, time of airblast arrival (sec)											
% of fireball energy emitted prior to T1											
% of fireball energy emitted in (T2-T1) sec											

Table III. Cont. . . .

Mesh point i	6	7	8	9	10	11	12	13	14	15	16
Maximum upward surface velocity (cm/sec)	0.23	0	0.16	2.8	2.3	4.1	4.7	9.8	12.2	16.7	27.6
T1, time of max velocity (sec)	0.0395	--	0.043	.0485	.0485	.0515	.0545	.0605	.0635	.0695	.0755
T2, time of airblast arrival (sec)	.0407	.0425	.0447	.0473	.0503	.0537	.0575	.0618	.0665	.0716	.0772
% of fireball energy emitted prior to T1	--	--	--	< 1	< 1	~ 1	~ 1	< 2	< 2	~ 2	~ 3
% of fireball energy emitted in (T2-T1) sec.	0	--	< 1	< 1	< 1	< 1	<1	< 1	< 1	< 1	< 1

Mesh point i	17	18	19	20	21	22	23	24	25	26	27
Maximum upward surface velocity (cm/sec)	27.7	32.4	32.1	35.3	35.1	34.2	32.9	33.3	33.0	29.8	27.6
T1, time of max velocity (sec)	.0815	.0875	.0935	.0995	.1055	.1115	.1175	.1235	.1295	.1355	.1415
T2, time of airblast arrival (sec)	.0832	.0885	.0939	.0997	.1059	.1125	.1195	.1268	.1346	.1427	.1511
% of fireball energy emitted prior to T1	~ 3	~ 3	~ 4	~ 5	~ 5	~ 5	~ 6	~ 7	~ 10	~ 11	~ 12
% of fireball energy emitted in (T2-T1) sec	~ 1	~ 1	< 1	< 1	< 1	< 1	~ 1	~ 1	~ 1	~ 1	~ 1

Table IV. Surface Velocity Data in Varied Ground Media - Run #2

Mesh point i	28	29	30	31	32	33	34	35	36	37	38
Maximum upward surface velocity (cm/sec)	23.0	20.1	18.0	17.3	16.3	15.2	14.9	14.2	13.4	13.0	13.3
T1, time of max velocity (sec)	.1475	.1535	.1595	.1655	.1715	.1775	.1865	.1925	.1985	.2045	.2105
T2, time of airblast arrival (sec)	.1599	.1691	.1786	.1884	.1986	.2041	.2199	.2311	.2425	.2543	.2664
% of fireball energy emitted prior to T1	~ 12	~ 15	~17	~ 17	~ 18	~19	~ 21	~ 22	~ 22	~ 23	~ 23
% of fireball energy emitted in (T2-T1) sec.	~ 2	~ 2	~ 2	~ 4	~ 4	~ 3	~ 4	~ 7	~ 9	~ 9	~10

Mesh point i	39	40	41	42							
Maximum upward surface velocity (cm/sec)	10.5	10.2	10.7	10.2							
T1, time of max velocity (sec)	.2195	.2255	.2285	.2345							
T2, time of airblast arrival (sec)	.2788	.2915	.3044	.3176							
% of fireball energy emitted prior to T1	~ 25	~ 28	~ 32	~ 32							
% of fireball energy emitted in (T2-T1) sec	~ 10	~ 11	~ 13	~ 13							

Table IV. Cont. . . .

Mesh point i	6	7	8	9	10	11	12	13	14	15	16
Maximum upward surface velocity (cm/sec)	0	0	0	0.22	0.14	0.37	0.38	0.79	1.10	1.30	2.76
T1, time of max velocity (sec)	--	--	--	.0455	.0485	.0515	.0545	.0575	.0635	.0695	.0755
T2, time of airblast arrival (sec)	.0407	.0425	.0447	.0473	.0503	.0537	.0575	.0619	.0665	.0715	.0772
% of fireball energy emitted prior to T1	--	--	--	< 1	< 1	~ 1	~ 1	< 2	< 2	~ 2	~ 3
% of fireball energy emitted in (T2-T1) sec.	--	--	--	< 1	< 1	< 1	< 1	< 1	< 1	< 1	< 1

Mesh point i	17	18	19	20	21	22	23	24	25	26	27
Maximum upward surface velocity (cm/sec)	3.30	3.30	3.7	4.5	6.4	4.34	4.5	8.0	7.7	8.4	14.2
T1, time of max velocity (sec)	.0815	.0875	.0935	.0995	.1055	.1115	.1175	.1265	.1325	.1445	.1505
T2, time of airblast arrival (sec)	.0832	.0885	.0939	.0997	.1059	.1125	.1195	.1268	.1346	.1427	.1511
% of fireball energy emitted prior to T1	~ 3	~ 3	~ 4	~ 5	~ 5	~ 5	~ 6	~ 8	~ 9	~ 13	~ 15
% of fireball energy emitted in (T2-T1) sec	~ 1	~ 1	< 1	< 1	< 1	< 1	~ 1	~ 1	< 1	--	< 1

Table V. Surface Velocity Data for Varied Ground Media - Run #3

Mesh point i	28	29	30	31	32	33	34	35	36	37	38
Maximum upward surface velocity (cm/sec)	16.3	17.8	17.8	16.2	15.3	13.7	12.2	11.2	10.3	9.7	9.1
T1, time of max velocity (sec)	.1595	.1685	.1775	.1835	.1925	.1985	.2015	.2075	.2165	.2195	.2285
T2, time of airblast arrival (sec)	.1599	.1691	.1786	.1884	.1986	.2041	.2199	.2311	.2425	.2543	.2664
% of fireball energy emitted prior to T1	~ 17	~ 18	~ 19	~ 20	~ 22	~ 22	~ 23	~ 23	~ 24	~ 25	~ 32
% of fireball energy emitted in (T2-T1) sec.	< 1	< 1	~ 1	~ 1	~ 2	~ 1	~ 2	~ 4	~ 3	~ 5	~ 8

Mesh point i	39	40	41	42							
Maximum upward surface velocity (cm/sec)	8.5	8.0	7.3	7.1							
T1, time of max velocity (sec)	.2315	.2375	.2435	.2495							
T2, time of airblast arrival (sec)	.2788	.2915	.3044	.3176							
% of fireball energy emitted prior to T1	~ 32	~ 33	~ 33	~ 34							
% of fireball energy emitted in (T2-T1) sec	~ 7	~ 8	~ 10	~ 10							

Table V. Cont. . . .

(Page intentionally left blank)

The stiff, uniform ground medium used in Run #2 produced the greatest vertical velocities. While initially appearing to conflict with Equation (1), this result is apparently due to the ability of the stiffer medium to transmit signals ahead of the airblast which were created "upstream" at higher overpressures, while these same signals are not able to outrun the airblast in the slower, more compressible medium of Run #1. Another factor is the ability of a stiffer medium to more readily transmit the higher frequency disturbances. These higher frequency components may, in part, explain the larger vertical velocities.

Because the heating from the fireball which any rising dust receives is of interest in creating the thermal layer which determines the precursor, Tables III-V also give data pertinent to the fireball radiation emission. Significant amount of fireball heating can be received by rising dust only when the difference between T1, the time of occurrence of maximum upward surface velocity, and T2, the time of airblast arrival, is sizeable. This will only occur when the seismic signal is able to substantially outrun the airblast. Such substantial outrunning is not reflected in the Tables III-V because the upward velocities continue to diminish with increasing ground range.

Dust layers created ballistically would reach a maximum height of only 0.096 cm for Run #1, 0.64 cm for Run #2, 0.16 cm for Run #3, and a negligible height for Run #4.

IV. Conclusions and Recommendations

Conclusions

Accuracy requirements, interference from artificially reflected signals, and computer storage limitations together prevented the comparison of results obtained with this model (rigid righthand and bottom mesh boundaries) with the available published data. The data on-hand consisted of independent, elastic calculations of late-time, airblast-induced ground motions and of late-time seismic motion data from actual test events.

Prevention of the artificially reflected signals and reduction of the computer storage requirements would have permitted this comparison. Application of the transmitting boundary condition constructed to accomplish the above two goals yielded indefinite results at best. This uncertainty in whether the transmitting boundary condition was properly constructed prohibited its use in validating the model against the independent data.

Thus, the model remains unvalidated, and data derived from it must be viewed accordingly. Nonetheless, it appears that several general conclusions can be made.

First, the surface velocities resulting from simulation of a 28 kiloton atmospheric burst at 500 feet height of burst yielded a dust layer ballistically reaching only 0.64 cm at its highest point for the stiff one-layer ground medium, 0.096 cm for the softer one-layer medium, and a negligible height for the more realistic four-layer Frenchman Flats medium. These heights are

significantly less than the two to three meter high dust layers known to exist prior to airshock arrival. Therefore, it must be concluded that as postulated (ballistic rise only) the airblast is not likely to significantly contribute to the precursor.

However, the magnitude of upward vertical velocities computed indicate that the seismic motions of the ground surface can be significant and should be considered in any modeling of thermal layer precursor generation. In particular, the seismic ground motions can alter the velocity with which dust is injected into the air by another causal mechanism such as the thermally-induced soil blow-off mechanism researched by AFWL. Only when another causal mechanism can be shown to occur sufficiently in advance of the arrival of the seismic signals to preclude the interaction of the two mechanisms does it appear that the airblast effect can be ignored.

In addition, AFWL modeling of the thermally-induced soil blow-off indicates that the injection velocity of the particles can range from 50 to 200 cm/sec without significantly altering the height of the dust layer computed by their model. At the maximum injection velocity of 200 cm/sec, the dust would ballistically rise only 20 cm — not the 2-3 meters found experimentally. This indicates that thermal radiation transport and hydrodynamics is the more dominant force lifting the dust particles. Redefining the airblast/seismic model to include these two effects may well result in airblast-induced thermal layers more nearly in agreement with experimental data. Or stated another way, the

key factor may be to begin the soil particles in an upward motion whereby the thermal radiation transport, hydrodynamics, and Taylor instabilities dominate to lift the soil to the significant heights of several meters. The role of airblast-induced vertical motions in the precursor formation certainly warrants further research. (Prentice, J., 1976: 13)

Finally, velocities imparted to the surface dust before and after arrival of the airshock may have considerable effect upon the amount of dust swept up as the airshock passes. This airborne dust would be expected to have significant impact upon the dynamic pressure and the erosive ability of the airshock.

Recommendations

Recommendations for further work with the computer model developed as an adjunct of this thesis research include:

1. the further search of published literature in an effort to find early-time seismic motion data with which the rigid boundary model may be validated;

2. the further search of published literature to find one or more suitable, generalized algorithms for peak overpressure and positive pressure phase duration; such algorithms would eliminate the requirement of generating a new surface pressure function for each new problem computed;

3. the further study, analytical development, and construction of a transmitting boundary; if successful, this work can have wide applications in this simulation as well as other models using a fixed finite difference mesh;

4. refinement of the model to confidently give arrival time data of the airblast-induced seismic motion.

Recommendations for further work on the airblast-induced precursor include:

1. the study of experiemental data to give time of occurrence of the thermal layer for comparison with seismic signal arrival times in order to determine whether the airblast-induced seismic signals arrive too late to significantly contribute to the thermal layer; and

2. if the above investigation reveals that the arrival of the seismic signals is not too late, incorporation of thermal radiation transport and hydrodynamics into the model.

Bibliography

Ganong, Maj. Gary P. Proposed Thesis Topic: Thermal Layer Model. (Correspondence with AFIT/ENP), 1978.

Glasstone, Samuel and Philip J. Dolan. The Effects of Nuclear Weapons. US DOD and US DE, 1977.

Hadala, P. F. Effect of Constitutive Properties of Earth Media on Outrunning Ground Shock from Large Explosions. US Army Engineer Waterways Experiment Station, Technical Report S-73-6, 1973.

Knasel, Michael T. Thermal Induced Blow-Off, A Report on Experimental Studies, Volume I. Science Applications, Inc., for Defense Nuclear Agency, DNA-3723F-1, 1975.

Kolsky, H. Stress Waves in Solids. Oxford: Clarendon Press, 1953.

Liner, Robert T., et. al. Nuclear Precursor Phenomenology and Sweep-Up Dust Cloud Model Development. Science Applications, Inc., for Defense Nuclear Agency, DNA-3781F, 1975.

Newmark, N. M. Air Force Design Manual: Principles and Practices for Design of Hardened Structures. AFSWC-TDR-62-138, 1962.

Nickel, George H., Professor of Physics, Air Force Institute of Technology. (private communication). WPAFB, Ohio, 1978.

Prentice, John K. and Burton S. Chambers, III. Sensitivity of AFWL Thermal Layer Preductions to Variations in Physical and Code Parameters. SAI-76-515-AQ, 1976.

Appendix A

One-Dimensional Estimate of the Maximum Vertical Velocity

Suppose that S_x, the displacement of a particle in the ground, can be expressed as a wave-like disturbance propagating in the x-direction with velocity c.

$$S_x = f(t-c/x) \tag{A-1}$$

The displacement S_x then satisfies the wave equation. This, of course, must be the case as stress within an elastic solid is known to be a generalized form of Hooke's Law. (Kolsky, 1953: 8)

This one-dimensional stress can be expressed as the following (Newmark, N., 1962: C-9)

$$\text{stress } \sigma_x = \rho c^2 \frac{\partial S_x}{\partial x} = \rho c^2 \frac{\partial f(t-x/c)}{\partial x} \tag{A-2}$$

where ρ is the density of the solid medium.

Differentiating the function f yields

$$\sigma_x = \rho c^2 \frac{\partial f(t-x/c)}{\partial x} = \rho c^2 \frac{\partial f(t-x/c)}{\partial (t-x/c)} \frac{\partial (t-x/c)}{\partial x}$$

$$= -\rho c \frac{\partial f(t-x/c)}{\partial (t-x/c)}$$

The boundary condition which applies at the surface x=0 is that the stress is equal to the normal loading of the pressure on the surface, or

$$\sigma_x \Big|_{x=0} = -\rho c \left. \frac{\partial f(t-x/c)}{\partial (t-x/c)} \right|_{x=0} = -P(t) \qquad \text{(A-3)}$$

However, the particle velocity is simply the derivation of the particle displacement with respect to time.

$$V_x = \frac{\partial S_x}{\partial t} = \frac{\partial f(t-x/c)}{\partial t}$$

$$= \frac{\partial f(t-x/c)}{\partial (t-x/c)} \quad \frac{\partial (t-x/c)}{\partial t} = \frac{\partial f(t-x/c)}{\partial (t-x/c)} \qquad \text{(A-4)}$$

Substituting for $\dfrac{\partial f}{\partial (t-x/c)}$ in Equation (A-3) gives

$$- c \rho V_x \Big|_{z=0} = -P(t)$$

or,

$$V_x \Big|_{z=c} = \frac{P(t)}{\rho c}$$

The particle velocity is a maximum when the loading pressure is a maximum. Finally,

$$\left[V_x \Big|_{z=0} \right]_{max} = \frac{P_o}{\rho c}$$

Appendix B

Effect of Ground Medium Layering on Stress (Newmark, 1962: C-13—C-15)

Given the following two-layered ground medium:

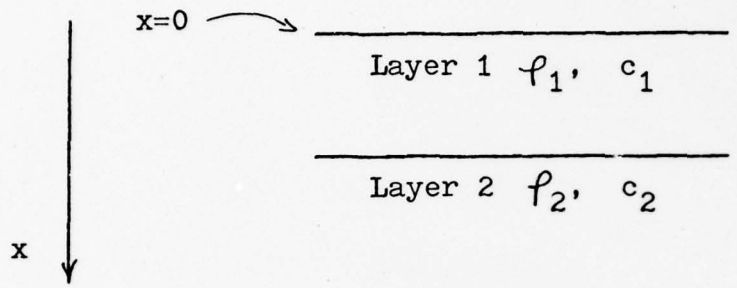

where ρ_i is the density of the ith layer, and

c_i is the seismic velocity of the ith layer.

If an elastic medium is assumed then the displacement of a particle within this solid must obey the wave equation,

$$\frac{\partial^2 S_x}{\partial t^2} = \rho c^2 \frac{\partial^2 S_x}{\partial x^2} .$$

Solutions to the wave equation take the form

$$S_x = f(t-x/c) + g(t+x/c)$$

where $f(t-x/c)$ represents a wave traveling in the positive x-direction, and

$g(t+x/c)$ represents a wave traveling in the negative x-direction.

Now consider a disturbance incident upon the interface between the two layers, namely,

$$S_x = f(t-x/c)$$

The stress incident upon the interface is given by

$$\sigma_{x_{incident}} = \rho_1 c_1^2 \frac{\partial S_x}{\partial x} = - \rho_1 c_1 \frac{\partial f}{\partial (t-x/c)} \qquad \text{(B-1)}$$

Let the incident wave or disturbance be expressed as the sum of reflected and transmitted components.

$$S_{x_{incident}} = S_{x_{reflected}} + S_{x_{transmitted}}$$

or, alternately,

$$f(t-x/c) = G(t+x/c) + F(t-x/c)$$

From Equation (B-1) the interface condition that the sum of reflected and transmitted stresses must equal the incident stress can be applied.

$$\sigma_{x_{incident}} = \sigma_{x_{reflected}} + \sigma_{x_{transmitted}}$$

or

$$\rho_1 c_1^2 \frac{\partial f(t-x/c)}{\partial x} = \rho_1 c_1^2 \frac{\partial G(t+x/c)}{\partial x} + \rho_2 c_2^2 \frac{\partial F(t-x/c)}{\partial x} \qquad \text{(B-3)}$$

Let

R = reflection coefficient = constant in time, and

T = transmission coefficient = constant in time.

such that $G(t+x/c_1) = R\, f(t-x/c_1)$ and

$F(t-x/c_2) = T\, f(t-x/c_1)$.

From (B-2), $f = Tf + Rf$

or,

$$1 - R = T.$$

From (B-1) and (B-3), $\rho_1 c_1^2 \frac{\partial f}{\partial x} = - \rho_1 c_1 \frac{\partial f}{\partial (t-x/c_1)}$

$$= - \rho_2 c_2 \frac{\partial F}{\partial (t-x/c_2)} + \rho_1 c_1 \frac{\partial G}{\partial (t-x/c_1)} \qquad \text{(B-5)}$$

However,

$$\frac{\partial f(t-x/c)}{\partial t} = \frac{\partial f(t-x/c)}{\partial (t-x/c_1)} \frac{\partial (t-x/c)}{\partial t} = \frac{\partial f}{\partial (t-x/c_1)} \qquad \text{(B-6)}$$

Applying (B-6) to Equation (B-5),

$$- \rho_1 c_1 \frac{\partial f}{\partial t} = - \rho_2 c_2 \, T \frac{\partial f}{\partial t} + \rho_1 c_1 \, R \frac{\partial f}{\partial t}$$

Dividing by $\left(- \rho_1 c_1\right)$,

$$1 = \left(\frac{\rho_2 c_2}{\rho_1 c_1}\right) T - R$$

$$1 + R = \left(\frac{\rho_2 c_2}{\rho_1 c_1}\right) T \qquad \text{(B-7)}$$

Combining (B-4) and (B-7) gives

$$2 = T\left(1 + \frac{\rho_2 c_2}{\rho_1 c_1}\right),$$

Finally,

$$T = \frac{2}{1 + \frac{\rho_2 c_2}{\rho_1 c_1}} \quad , \tag{B-8}$$

and

$$R = \frac{\frac{\rho_2 c_2}{\rho_1 c_1} - 1}{\frac{\rho_2 c_2}{\rho_1 c_1} + 1} \tag{B-9}$$

since $G = Rf$, $\frac{\partial G}{\partial t} = R \frac{\partial f}{\partial t}$

but

$$\frac{\partial G(t+x/c)}{\partial (t+x/c)} \frac{\partial (t+x/c)}{\partial t} = R \frac{\partial f(t-x/c)}{\partial (t-x/c)} \frac{\partial (t-x/c)}{\partial t}$$

giving

$$\rho_1 c_1 \frac{\partial G}{\partial (t+x/c)} = \rho_1 c_1 R \frac{\partial f}{\partial (t-x/c)} \quad .$$

or, equivilently,

$$\sigma_r = R \sigma_i \quad . \tag{B-10}$$

Similarly,

$$F = Tf$$

$$\frac{\partial F}{\partial t} = T\frac{\partial f}{\partial t} \Rightarrow \frac{\partial F}{\partial (t-x/c_2)} \quad \frac{\partial (t-x/c_2)}{\partial t}$$

$$= T \frac{\partial f}{\partial (t-x/c_2)} \quad \frac{\partial (t-x/c_1)}{\partial t}$$

or,

$$\frac{\partial F}{\partial (t-x/c_2)} = T \frac{\partial f}{\partial (t-x/c_1)}$$

Continuing similar to the derivation for (B-10) gives

$$\sigma_T = \frac{2}{\frac{\rho_1 c_1}{\rho_2 c_2} + 1} \quad \sigma_i \qquad \text{(B-11)}$$

Consider what happens if this transmitted stress σ_T is allowed to be incident upon the interface. The stress transmitted back to the upper layer σ_T' is given by

$$\sigma_T' = \frac{2}{\frac{\rho_2 c_2}{\rho_1 c_1} + 1} \quad \sigma_T = \frac{2}{\frac{\rho_2 c_2}{\rho_1 c_1} + 1} \left\{ \frac{2}{\frac{\rho_1 c_1}{\rho_2 c_2} + 1} \right\} \sigma_i$$

$$= \frac{4}{2 + \frac{\rho_1 c_1}{\rho_2 c_2} + \frac{\rho_2 c_2}{\rho_1 c_1}} \quad \sigma_i$$

If $\rho_2 c_2 > \rho_1 c_1$, then

$$\frac{\rho_2 c_2}{\rho_1 c_1} > 1 .$$

Thus,

$$\sigma_T = \frac{4}{2 + \frac{\rho_1 c_1}{\rho_2 c_2} + \frac{\rho_2 c_2}{\rho_1 c_i}} \sigma_i$$

and $\sigma_T \geq \sigma_i$ for

$$\frac{\rho_1 c_1}{\rho_2 c_2} + \frac{\rho_2 c_2}{\rho_1 c_1} < 2 .$$

Appendix C

Derivation of Algorithm for Decay of Overpressure with Time

To accurately apply the overpressure on the ground surface requires that its time-dependent behavior be incorporated. Accurate behavior with time is necessary to couple the correct frequency components of the airblast into the ground. To this end, it is undertaken to transform the data contained in Glasstone's, The Effects of Nuclear Weapons, and presented in Figure 17 into an algorithm which could then be incorporated into the computer model.

It is first observed that the data curves are very nearly symmetric about the line indicated in the figure. Next, a "super ellipse" of the following form and centered at the point (1,1) is argued to reasonably fit the curves (Nickel, 1978):

$$(1-x)^m + (1-y)^m = 1 \qquad \text{(C-1)}$$

At the symmetry axis chosen, x=y. Or, in this application

$$P(t)/PEAKP = t/t_p^+$$

where $P(t)$ = pressure at time t,

$PEAKP$ = peak overpressure,

t = time measured from arrival of shock front, and

t_p^+ = direction of positive overpressure phase.

At the symmetry axis Equation (C-1) becomes

$$(1-x)^m = \frac{1}{2} ,$$

from which results

$$m = \frac{\ln 2}{\ln (1-x)} . \qquad (C-2)$$

From Figure 17 data and Equation (C-2), the following table results:

PEAKP	$x = t/t_p^+$	1-x	m
20	.35	.65	1.60
100	.27	.73	2.20
200	.21	.79	2.94
1000	.12	.88	5.42

After several trials, the above table data relating PEAKP and m is chosen to be fit by a cubic equation in (ln PEAKP),

$$m = 1 + A * \ln \text{PEAKP} + B * (\ln \text{PEAKP})^2 + C * (\ln \text{PEAKP})^3 \qquad (C-3)$$

Three equations are set up using Equation (C-3) and the data table, then solved, giving

$A = 0.382,$

$B = -0.136,$ and

$C = 0.025$.

Knowing m, Equation (C-1) is solved for y yielding

$$y = 1 - \left[1 - (1-x)^m \right]^{1/m} ,$$

or equivalently,

$$\frac{P(t)}{PEAKP} = 1 - \left[1 - (1-t/t_p^+)^m \right]^{1/m} .$$

The results of using this curve-fitting algorithm are given in Figure 18 for the surface overpressure from a 28 kiloton event at 500 feet height of burst.

Figure 17. Rate of Decay of Overpressure with Time (Glasstone, 1977: 100)

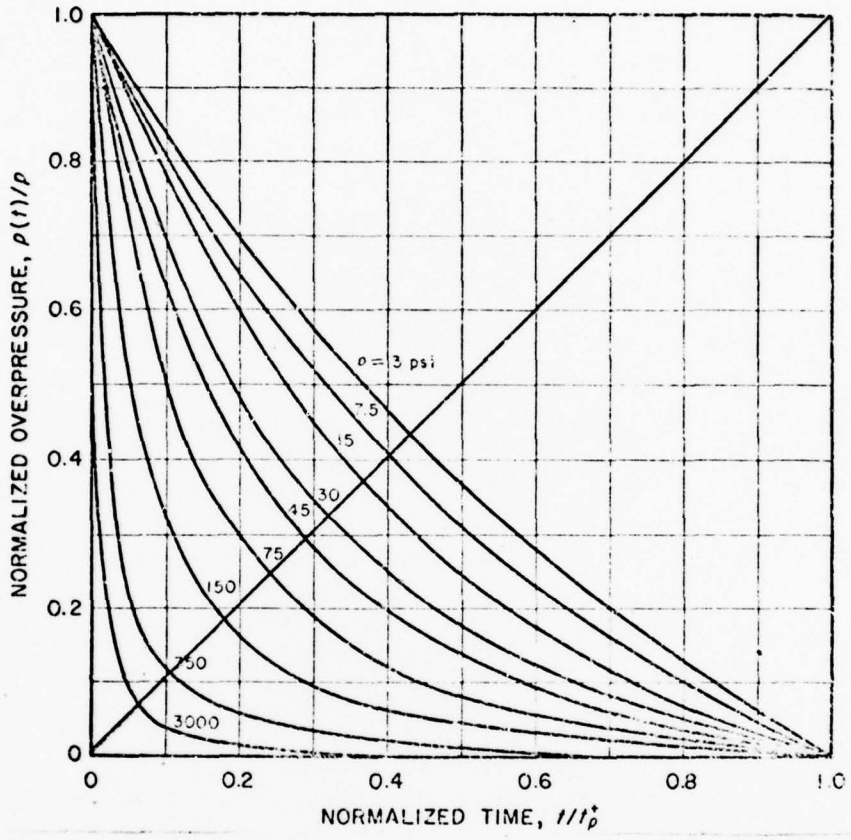

Figure 18. Comparison of Algorithm for Time-Dependent Overpressure and Glasstone Data

PEAKP	$\frac{t}{t_p^+}$	$\frac{P(t)}{PEAKP}$ algorithm	Glasstone
1563	0.071	0.142	0.14
1563	0.030	0.017	0.01
375	0.07	0.31	0.32
375	0.23	0.12	0.11

Appendix D

Derivation of a Transmitting Boundary

At a boundary it may be desirable to pass or transport seismic signals through the edge of the mesh as though a semi-infinite expanse of ground material existed beyond that edge. Although several conditions may exist upon which such a "transmitting" boundary can be constructed, an argument based upon momentum transfer is chosen.

Consider the finite difference mesh near such an edge, in this case, the bottom.

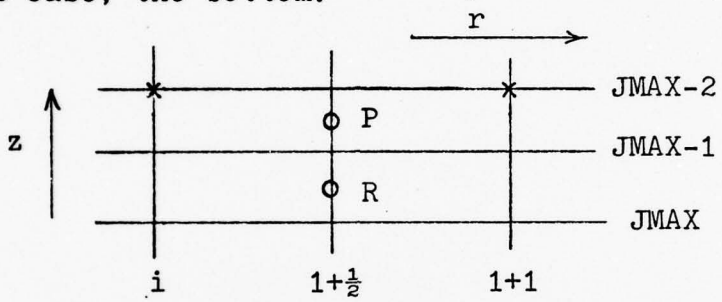

Assume that the horizontal level JMAX-1 is the boundary across which seismic signals are desired to be transmitted without reflection. The points marked with the symbol "X" are known. Thus, the stresses σ_{zz} and σ_{rz} can be calculated at point P, centered at (i+½, JMAX-3/2).

The stress σ_{zz} represents the flux of z-momentum in the z-direction, and σ_{rz} the flux of r-momentum in the z-direction. A properly constructed transmitting boundary would permit the outflow of positive momentum and the inflow of negative momentum, while preventing the inflow of positive momentum and outflow of negative momentum which result in a net increase in momentum flowing into the finite difference mesh.

The z-momentum density is given by the product ρV_z, and, similarly, the r-momentum density by ρV_r, where V_z and V_r are the velocities of the ground particles in the z-direction and r-direction, respectively. Assuming the density ρ to be constant near the mesh boundary of interest, the positiveness or negativeness of z- and r-momentum can be determined by testing the sign of the V_z and V_r velocity respectively.

Then, consider the following:

$$V_z = \frac{dS_z}{dt} = \frac{dS_z}{dz} \quad \frac{dz}{dt} \quad .$$

where S_z is the displacement of the bround in the z-direction.

Here $\frac{dz}{dt}$ is assumed to be greater than or equal to zero.

The following logic tables result:

$\frac{\partial S_z}{\partial z}\Big\|_p$	$\sigma_{zz}\Big\|_p$	indicate reflection ?	action
> 0	> 0	Yes	$\sigma_{zz}\Big\|_R = 0$
> 0	< 0	No	$\sigma_{zz}\Big\|_R = \sigma_{zz}\Big\|_p$
< 0	> 0	No	$\sigma_{zz}\Big\|_R = \sigma_{zz}\Big\|_p$
< 0	< 0	Yes	$\sigma_{zz}\Big\|_R = 0$

$\left.\frac{\partial S_r}{\partial r}\right\|_P$	$\left.\sigma_{rz}\right\|_P$	indicate reflection ?	action
> 0	> 0	Yes	$\left.\sigma_{rz}\right\|_R = 0$
> 0	< 0	No	$\left.\sigma_{rz}\right\|_R = \left.\sigma_{rz}\right\|_P$
< 0	> 0	No	$\left.\sigma_{rz}\right\|_R = \left.\sigma_{rz}\right\|_P$
< 0	< 0	Yes	$\left.\sigma_{rz}\right\|_R = 0$

When $\left.\frac{\partial S_z}{\partial z}\right|_P$, $\left.\frac{\partial S_r}{\partial r}\right|_P$, $\left.\sigma_{zz}\right|_P$, or $\left.\sigma_{rz}\right|_P$ is equal to zero, either action results in the same thing.

```
      PROGRAM THERMAL(INPUT,OUTPUT)                                      RNP 78
      DIMENSION Y(100,25,3),Z(100,25,3)                                  RNP 78
      DIMENSION AZP(100),BZP(100),CZP(100),DZP(100),P(100)               RNP 78
      DIMENSION AL(100,21)                                               GHN 78
      DIMENSION R(100)                                                   RNP 78
      DIMENSION  LAM(100,25), MU(100,25), RHO(100,25)                    RNP 78
      REAL LAM,MU,HOB                                                    RNP 78
      INTEGER RPLOT,ZPLOT                                                RNP 78
CC
CC
CC       GHN 78 INDICATES CODE GENERATED BY MAJOR GEORGE NICKEL FOR A     RNP 78
CC              CARTESIAN COORDINATE SEISMIC PROBLEM (VALLEY) IN 1978     RNP 78
CC              GHN IMPLIES SLIGHT CHANGE MADE TO VARIABLES/CONSTANTS IN  RNP 78
CC              NICKEL'S CODE                                             RNP 78
CC
CC       RNP 78 INDICATES CODE CHANGED OR ADDED BY CAPT RICHARD PRICE     RNP 78
CC              TO  NICKEL'S CARTESIAN CODE IN ORDER TO PERFORM SEISMIC   RNP 78
CC              CALCULATIONS IN CYLINDRICAL GEOMETRY (PRECURSOR)          RNP 78
CC
CC
CCCCCC
CCCCCC   INITIAL DATA                                                     GHN 78
CCCCCC
      READ*,YIELD,HOB,TZERO,RZERO,ZZERO,C,ALAM,AMU,ARHO,DEPTHA,BLAM,     RNP 78
     $ BMU,BRHO,DEPTHB,CLAM,CMU,CRHO,DEPTHC,DLAM,DMU,DRHO,DY,DZ,DT,IMAX, RNP 78
     $ JMAX,TWRITE,JWRITE,IFLAG,JFLAG,RPLOT,ZPLOT                       RNP 78
      PRINT 991                                                          RNP 78
  991 FORMAT("1PROBLEM --  SEISMIC CONTRIBUTOR TO NUCLEAR AIR BLAST PREC RNP 78
     $URSOR")                                                           RNP 78
      PRINT 992,YIELD,HOB                                                RNP 78
  992 FORMAT ("0 YIELD(MT)  ",E10.3," ,    HEIGHT OF BURST(CM) ",E12.5) RNP 78
      PRINT 993,TZERO                                                    RNP 78
  993 FORMAT("0 TZERO = TIME AFTER BURST AT WHICH CALCULATION IS STARTED RNP 78
     $ (SEC)= ",F8.4)                                                   RNP 78
      PRINT 994,RZERO                                                    RNP 78
```

```
 99?   FORMAT("0 RZERO= GROUND DISTANCE FROM GROUND ZERO AT WHICH SHOCK I RNP 78
     $S ASSUMED TO BE AT TZERO = ",E12.4,"  (CM)")                        RNP 78
       PRINT 99?,RZERO                                                    RNP 7
 99?   FORMAT("0 PZERO= AMBIENT PRESSURE BEFORE SHOCK ARRIVAL",E12.4,     RNP 78
     $ " (DYNES/CM**2)")                                                  RNP 78
       PRINT 99?,C                                                        RNP 78
 99?   FORMAT("0 C = SPEED OF SOUND IN  AMBIENT  AIR",E12.4,"  CM/SEC")   RNP 78
       PRINT  99?,DEPTH?,DEPTHB,DEPTHC                                    RNP 78
 99?   FORMAT("0 GROUND CONSTANTS:  DEPTHS OF LAYERS ARE (CM) ",3(E12.3)) RNP 78
       PRINT 99?                                                          RNP 78
 99?   FORMAT("  CAUTION *** DEPTHS ARE NOT WIDTHS OF LAYERS, BUT ACTUAL  RNP 78
     $DISTANCES THAT LAYER INTERFACES ARE LOCATED UNDER GROUND")           RNP 78
       PRINT 999,ALAM,AMU,ARHO                                            RNP 78
 99?   FORMAT("0 UPPER SOIL LAYER, LAMDA =  (DYNES/CM**2)  ",E12.3,",  MU RNP 78
     $ (DYNES/CM**2) =  ",E12.3,",  DENSITY(GM/CM**3)= ",E10.3)           RNP 78
       PRINT 1000,BLAM,BMU,BRHO                                           RNP 78
1000   FORMAT("0 SECOND SOIL LAYER,LAMDA==  (DYNES/CM**2)  ",E12.3,",  MU RNP 78
     $ (DYNES/CM**2) =  ",E12.3,",  DENSITY(GM/CM**3)= ",E10.3)           RNP 78
       PRINT 1001,CLAM,CMU,CRHO                                           RNP 78
1001   FORMAT("0 THIRD SOIL LAYER, LAMDA =  (DYNES/CM**2)  ",E12.3,",  MU RNP 78
     $ (DYNES/CM**2) =  ",E12.3,",  DENSITY(GM/CM**3)= ",E10.3)           RNP 78
       PRINT 1002,DLAM,DMU,DRHO                                           RNP 78
1002   FORMAT("0 FOURTH SOIL LAYER,LAMDA==  (DYNES/CM**2)  ",E12.3,",  MU RNP 78
     $ (DYNES/CM**2) =  ",E12.3,",  DENSITY(GM/CM**3)= ",E10.3)           RNP 78
       PRINT 1003,DY,DZ,DT,IMAX,JMAX                                      RNP 78
1003   FORMAT("0 CALCULATIONAL PARAMETERS, DY(CM) = ",E10.3,"  DZ (CM) =  RNP 78
     $  ",E10.3,  "  DT (SEC) =  ",E6.4,"  IMAX = ",I3,"  JMAX = ",I3)   RNP 78
       PRINT 1004,TWRITE                                                  RNP 78
1004   FORMAT("0 TWRITE = TIME TO BEGIN PRINT-OUT=",F6.3," SEC",//)       957 78
C                                                                         RNP
C                                                                         RNP 78
C                                                                         RNP 78
C         YIELD = BURST YIELD IN MT                                       RNP 78
C         HOB = HEIGHT OF BURST                                           RNP 78
C         TZERO= TIME OF SHOCK ARRIVAL AT RZERO (GLASSTONE OR DNA3781F)   RNP 78
C         T = 0  IS TIME OF BURST                                         RNP 78
```

AD-A063 934 AIR FORCE INST OF TECH WRIGHT-PATTERSON AFB OHIO SCH--ETC F/G 18/3
THE NUCLEAR AIR-SHOCK PRECURSOR: A STUDY OF THE CONTRIBUTION OF--ETC(U)
DEC 78 R N PRICE

UNCLASSIFIED AFIT/GNE/PH/78D-21 NL

2 OF 2
AD A063934

END
DATE FILMED
3-79
DDC

```
C       RZERO IS GROUND RANGE AT WHICH IT IS DESIRED TO START PROBLEM:   RNP 78
C             R NOT EQUAL ZERO NEGATES ALL PRESSURE IMPULSE PRIOR TO     RNP 78
C             RZERO: USE IN CONJUNCTION WITH PROPER TZERO                RNP 78
C       PZERO = AMBIENT PRESSURE                                         RNP 78
C       C = SOUND SPEED IN AMBIENT AIR                                   RNP 78
C       LAM,   MU, AND  RHO ARE ELASTIC CONSTANTS AND DENSITY OF GROUND  RNP 78
C           FOR CALCULATIONAL PURPOSES                                   RNP 78
C       ALAM,AMU,ARHO ARE PROPERTIES OF UPPERMOST SOIL LAYER             RNP 78
C       BLAM,BMU,BRHO ARE PROPERTIES OF SECOND SOIL LAYER                RNP 78
C       CLAM,CMU,CRHO ARE PROPERTIES OF THIRD SOIL LAYER                 RNP 78
C       DLAM,DMU,DRHO ARE PROPERTIES OF FOURTH SOIL LAYER                RNP 78
C       DY = RADIAL CELL WIDTH ; DZ = VERTICAL CELL WIDTH; (CM)          RNP 78
C       DT = TIME INCREMENT FOR CALCULATION                              RNP 78
C       IMAX = MAX RADIAL MESH PTS;  JMAX = MAX VERTICAL MESH PTS        RNP 78
C       TWRITE = TIME TO BEGIN PRINTOUT                                  RNP 78
C       JWRITE IS THE HORIZONTAL MESH LEVEL WHICH IS DESIRED TO BE       RNP 78
C             OUTPUT: J=2 IS SURFACE AND J=JMAX IS BOTTOM                RNP 78
C             OF MESH GRID                                               RNP 78
C       IFLAG = 0 MEANS DO NOT PRINT OUT Y ARRAY WHICH CORRESPONDS TO    RNP 78
C             PLOT: ANY NON-ZERO INTEGER GIVES PRINTOUT OF Y ARRAY       RNP 78
C       JFLAG = 0 MEANS DO NOT PRINT OUT Z ARRAY WHICH CORRESPONDS TO    RNP 78
C             PLOT: ANY NON-ZERO INTEGER GIVES PRINTOUT OF Z ARRAY       RNP 78
C       RPLOT = 0 IMPLIES DO NOT PLOT DISPLACEMENTS IN R-DIRECTION       RNP 78
C       ZPLOT = 0 IMPLIES DO NOT PLOT DISPLACEMENTS IN Z-DIRECTION       RNP 78
C
C
C       Z(I,J,T) = DISPLACEMENT OF SOIL IN VERTICAL DIRECTION AT TIME    RNP 78
C             T ABOUT ITS EQUILIBRIUM MESH POSITION I,J                  RNP 78
C       Y(I,J,T) = DISPLACEMENT OF SOIL IN  RADIAL  DIRECTION AT TIME    RNP 78
C             T ABOUT ITS EQUILIBRIUM MESH POSITION I,J                  RNP 78
C       I   INDICATES RADIAL POSITION IN FINITE DIFFERENCE MESH:         RNP 78
C             I = 2 IS AXIS OF SYMMETRY, IE., R=0                        RNP 78
C       R IS POSITIVE TO THE RIGHT, AND I INCREASES TO THE RIGHT         RNP 78
C       J   INDICATES VERTICAL POSITION IN FINITE DIFFERENCE MESH:       RNP 78
C             J = 2 IS GROUND SURFACE, IE., Z=0                          RNP 78
C       Z IS POSITIVE UPWARD, BUT J VALUES INCREASE DOWNWARD             RNP 78
```

```
      LAST = 1                                                          GHN 78
      NOW = 2                                                           GHN 78
      NEXT = 3                                                          GHN 78
      IMM = IMAX -1                                                     GHN 78
      JMM = JMAX - 1
      IM3 = IMAX - 3                                                    RNP 78
      T = TZERO                                                         RNP 78
C
C        VEL IS SHUTDOWN MECHANISM TO PREVENT REFLECTION FROM RIGHTHAND  RNP 78
C             BOUNDRY OF MESH; THUS, WE USE FASTEST SEISMIC VELOCITY    RNP 78
C
      LAMMAX = AMAX1(ALAM,BLAM,CLAM,DLAM)                               RNP 78
      MUMAX = AMAX1(AMU,BMU,CMU,DMU)                                    RNP 78
      RHOMAX = AMAX1(ARHO,BRHO,CRHO,DRHO)                               RNP 78
      VEL = SQRT((LAMMAX + 2.*MUMAX)/RHOMAX)                            RNP 78
C
C
C        DEFINE SOIL SEISMIC PROPERTIES
C        LAYER= LOCATION OF DEEPEST MESH VALUE Z WITH PROPERTIES OF A    RNP 78
C                GIVEN SOIL LAYER, 1E-1 TERM SOLVES PROBLEM OCCURRING    RNP 78
C                WHEN DEPTH/DZ IS EXACTLY AT SOME LEVEL J=N              RNP 78
C
C
      LAYERA = (DEPTHA/DZ - (1.E-4)*DZ) + 2                             RNP 78
      IF(LAYERA.GE.(JMAX-3)) PRINT 1070                                 RNP 78
 1070 FORMAT("0 CAUTION ****  FIRST LAYER INTERFACE LIES WITHIN OR BELOW RNP 78
     $ FRICTION REGION: REFLECTION FROM THE INTERFACE MAY BE INHIBITED") RNP 78
      IF(LAYERA.GT.JMAX) PRINT 1090                                     RNP 78
 1090 FORMAT("0 CAUTION ---  UPPER LAYER EXCEEDS MESH DEPTH  ")         RNP 78
      IF(LAYERA.GT.JMAX) LAYERA=JMAX                                    RNP 78
      LAYERA1=LAYERA + 1                                                RNP 78
      LAYERB = (DEPTHB/DZ - (1.E-4)*DZ) + 2                             RNP 78
      IF(LAYERB.GE.(JMAX-3)) PRINT 1080                                 RNP 78
```

```
1090 FORMAT("0 CAUTION **** SECOND LAYER INTERFACE LIES WITHIN OR BELOW RNP 78
     $ FRICTION REGION: REFLECTION FROM THE INTERFACE MAY BE INHIBITED") RNP 78
      IF(LAYERB.GT.JMAX) PRINT 1098                                     RNP 78
1098 FORMAT("0 CAUTION --- SECOND LAYER EXCEEDS MESH DEPTH  ")          RNP 78
      IF(LAYERB.GT.JMAX) LAYERB=JMAX                                    RNP 78
      LAYERB1=LAYERB + 1                                                RNP 78
      LAYERC = (DEPTHC/DZ - (1.E-4)*DZ) + 2                             RNP 78
      IF(LAYERC.GE.(JMAX-5)) PRINT 1070                                 RNP 78
1070 FORMAT("0 CAUTION ****  THIRD LAYER INTERFACE LIES WITHIN OR BELOW RNP 78
     $ FRICTION REGION: REFLECTION FROM THE INTERFACE MAY BE INHIBITED") RNP 78
      IF(LAYERC.GT.JMAX) PRINT 1097                                     RNP 78
1097 FORMAT("0 CAUTION ---  THIRD LAYER EXCEEDS MESH DEPTH  ")          RNP 78
      IF(LAYERC.GT.JMAX) LAYERC=JMAX                                    RNP 78
      LAYERC1=LAYERC + 1                                                RNP 78
      DO 1110 I=2,IMAX                                                  RNP 78
      DO 1100 J=2,LAYERA                                                RNP 78
       LAM(I,J) = ALAM                                                  RNP 78
       MU(I,J) = AMU                                                    RNP 78
      RHO(I,J) = ARHO                                                   RNP 78
1100 CONTINUE                                                           RNP 78
      IF(LAYERA.GE.JMAX) GO TO 1110                                     RNP 78
      DO 1102 J=LAYERA1,LAYERB                                          RNP 78
       LAM(I,J) = BLAM                                                  RNP 78
       MU(I,J) = BMU                                                    RNP 78
      RHO(I,J) = BRHO                                                   RNP 78
1102 CONTINUE                                                           RNP 78
      IF(LAYERB.GE.JMAX) GO TO 1110                                     RNP 78
```

```
      DO 1103 J=LAYERO1,LAYERO                                          RNP 78
       LAM(I,J) = CLAM                                                  RNP 78
       MU(I,J) = CMU                                                    RNP 78
      RHO(I,J) = CRHO                                                   RNP 78
 1103 CONTINUE                                                          RNP 78
      IF(LAYERO.GE.JMAX) GO TO 1110                                     RNP 78
      DO 1104 J=LAYERO1,JMAX                                            RNP 78
       LAM(I,J) = DLAM                                                  RNP 78
       MU(I,J) = DMU                                                    RNP 78
      RHO(I,J) = DRHO                                                   RNP 78
 1104 CONTINUE                                                          RNP 78
 1110 CONTINUE                                                          RNP 78
CCCCC
CCCCCC   INITIALIZE THE MESH VALUES                                     GHN 78
CCCCC
      DO 4 I=1,IMAX                                                     GHN 78
      DO 4 J=1, JMAX                                                    GHN 78
    3 Y(I,J,1) = 0.                                                     GHN 78
      Y(I,J,2) = 0.                                                     GHN 78
      Y(I,J,3) = 0.                                                     GHN 78
      Z(I,J,1) = 0.                                                     GHN 78
      Z(I,J,2) = 0.                                                     GHN 78
      Z(I,J,3) = 0.                                                     GHN 78
      R(I) = DY*(I-2)      + RZERO                                      RNP 78
    4 CONTINUE                                                          GHN 78
CCCCCC
CCCCCC   RETURN POINT FOR NEW TIME STEP IS STATEMENT 5                  GHN 78.
CCCCCC
    5 CONTINUE                                                          GHN 78.
```

```
CCCCCC
CCCCCC   SURFACE PRESSURE                                              GHN 78
CCCCCC
      DO 6 I=2,IMAX                                                    RNP 78
      P(I) = PRESS(YIELD,RHO,T,R(I),R ERO,YYSHOCK)                     RNP 78
C
C        YYSHOCK LOCATES THE LEADING EDGE OF SHOCK FRONT ON THE GROUND  RNP 78
C
    6 CONTINUE                                                         GHN 78
CCCCCC
CCCCCC   BOUNDARY CONDITIONS                                           GHN 78
CCCCCC
      DO 7 I=3,I1M                                                     RNP 78
      IF(R(I).EQ.0.) PRINT 1005                                        RNP 78
 1005 FORMAT("0 R(I) = 0 : WHICH IMPLIES DIVISION BY ZERO")            RNP 78
      Y(I,1,NOW)=Y(I,3,NOW)+DZ/DY*(Z(I-1,2,NOW)-Z(I+1,2,NOW))          GHN 78
      Z(I,1,NOW)=Z(I,3,NOW)-2.*(DZ/(  LAM(I,2)+2.* MU(I,2)  ))*        GHN*78
     1   (P(I)+(  LAM(I,2)/(2.*DY))*(Y(I+1,2,NOW)-Y(I-1,2,NOW)))       GHN*78
     $   -(Y(I,2,NOW)* LAM(I,2)/(R(I)))*(2.*DZ/( LAM(I,2)+2.* MU(I,2)) ) RNP 78
    7 CONTINUE                                                         GHN 78
      DO 8 J=1,JMAX                                                    GHN 78
      Y(1,J,NOW) =-Y(3,J,NOW)                                          GHN 78
      Z(1,J,NOW)=Z(3,J,NOW)                                            GHN 78
      Y(2,J,NOW) = 0.0                                                 RNP 78
      Z(2,J,NOW) = Z(3,J,NOW)                                          RNP 78
    8 CONTINUE                                                         GHN 78
CCCCCC
CCCCCC   INITIALIZE FIRST DIFFERENCES                                  GHN 78
```

```
CCCCCC
      J = 1
      DO 9 I=3,IMN                                                    RNP 78
      AZP(I) = (Y(I+1,J+1,NOW) + Y(I+1,J,NOW) - Y(I-1,J+1,NOW)
     1   - Y(I-1,J,NOW))/(4.*DY)
      BZP(I) = (Y(I,J,NOW) - Y(I,J+1,NOW))/DZ
      CZP(I) = (Z(I+1,J,NOW) + Z(I+1,J+1,NOW) - Z(I-1,J,NOW)
     1   - Z(I-1,J+1,NOW))/(4.*DY)
      DZP(I) = (Z(I,J,NOW) - Z(I,J+1,NOW))/DZ
    9 CONTINUE
CCCCCC
CCCCCC   MAIN DIFFERENCE EQUATIONS                                    GHN 78
CCCCCC
      DO 10 J=2,JMN
      I = 1
      APZ = (Y(I+1,J,NOW) - Y(I,J,NOW))/DY
      BPZ = (Y(I,J-1,NOW) + Y(I+1,J-1,NOW) - Y(I,J+1,NOW)
     1   -Y(I+1,J+1, NOW))/(4.*DZ)
      CPZ = (Z(I+1,J,NOW) - Z(I,J,NOW))/DY
      DPZ = (Z(I,J-1,NOW)+Z(I+1,J-1,NOW) - Z(I,J+1,NOW) - Z(I+1,J+1,
     1   NOW))/(4.*DZ)
      DO 10 I=3,IMM                                                   RNP 78
      IF(R(I).EQ.0.) PRINT 1005                                       RNP 78
      AMZ = APZ
      BMZ = BPZ
       CMZ = CPZ
      DMZ = DPZ
```

```
 APZ = (Y(I+1,J,NOW) - Y(I,J,NOW))/DY
 BPZ = (Y(I,J-1,NOW) + Y(I+1,J-1,NOW) - Y(I,J+1,NOW)
1    -Y(I+1,J+1, NOW))/(4.*DZ)
 CPZ = (Z(I+1,J,NOW) - Z(I,J,NOW))/DY
 DPZ = (Z(I,J-1,NOW)+Z(I+1,J-1,NOW) - Z(I,J+1,NOW) - Z(I+1,J+1,
1    NOW))/(4.*DZ)
 AZM = AZP(I)
 BZM = BZP(I)
 CZM = CZP(I)
 DZM = DZP(I)
 AZP(I) = (Y(I+1,J+1,NOW) + Y(I+1,J,NOW) - Y(I-1,J+1,NOW)
1    - Y(I-1,J,NOW))/(4.*DY)
 BZP(I) = (Y(I,J,NOW) - Y(I,J+1,NOW))/DZ
 CZP(I) = (Z(I+1,J,NOW) + Z(I+1,J+1,NOW) - Z(I-1,J,NOW)
1    - Z(I-1,J+1,NOW))/(4.*DY)
 DZP(I) = (Z(I,J,NOW) - Z(I,J+1,NOW))/DZ
 Y(I,J,NEXT) = 2.*Y(I,J,NOW) - Y(I,J,LAST)                              GHN 78
1    +DT*DT/RHO(I,J)*(((  LAM(I,J) +  LAM(I+1,J) )*(APZ + DPZ)         GHN*78
2    - (  LAM(I,J) +  LAM(I-1,J) )*(AMZ + DMZ))/(2.*DY)                GHN*78
3    + ((  MU(I,J)  +  MU(I+1,J)  )*APZ                                GHN*78
4    - (  MU(I,J)  +  MU(I-1,J)  )*AMZ)/DY                             GHN*78
5    + ((  MU(I,J)  +  MU(I,J-1)  )*(BZM + CZM)                        GHN*78
6    - (  MU(I,J+1)  +  MU(I,J) )*(BZP(I) + CZP(I)))/(2.*DZ))          GHN*78
A    +(DT*DT/RHO(I,J))*(((.5*(LAM(I,J)+LAM(I+1,J))+(MU(I,J)+           RNP 78
B   MU(I+1,J)))/DY)*((Y(I,J,NOW)+Y(I+1,J,NOW))/(2.*DY*(I-1.5)))-((     RNP 78
C .5*(LAM(I,J) + LAM(I-1,J)) + (MU(I,J) + MU(I-1,J)))/DY)*             RNP 78
D ((Y(I,J,NOW) + Y(I-1,J,NOW))/(2.*DY*(I-2.5))))                       RNP 78
 Z(I,J,NEXT) = 2.*Z(I,J,NOW) - Z(I,J,LAST)                             GHN 78
1    + DT*DT/RHO(I,J)*(((  LAM(I,J-1) +  LAM(I,J) )*(AZM + DZM)        GHN*78
2    - (  LAM(I,J+1) +  LAM(I,J) )*(AZP(I) + DZP(I)))/(2.*DZ)          GHN*78
```

```
     3   + ((  MU(I,J-1)  +  MU(I,J)  )*DZM                                  GHN*78
     4   - (  MU(I,J)  +  MU(I,J+1)  )*DZP(I))/DZ                            GHN*78
     5   + ((  MU(I,J)  +  MU(I+1,J)  )*(BMZ + BPZ)                          GHN*78
     6   - (  MU(I,J)  +  MU(I-1,J)  )*(BMZ + BMZ))/(2.*DY))                 GHN*78
     A + (DT*DT/RHO(I,J))*(((.5*( LAM(I,J)+  LAM(I,J-1)) +  MU(I,J) +        RNP 78
     B   MU(I,J-1))/DZ)*((Y(I,J,NOW) + Y(I,J-1,NOW))/(2.*R(I))) - ((.5*      RNP 78
     C  ( LAM(I,J) +  LAM(I,J+1)) +  MU(I,J) +  MU(I,J+1))/DZ)*((Y(I,J,      RNP 78
     D   NOW) + Y(I,J+1,NOW))/(2.*R(I)))                                      RNP 78
     E -( MU(I,J)/R(I))*(((Y(I,J,NOW)+Y(I,J-1,NOW))/(2.*DZ)) - ((Y(I,J,       RNP 78
     F   NOW) + Y(I,J+1,NOW))/(2.*DZ)) - ((Z(I,J,NOW) + Z(I+1,J,NOW))/        RNP 78
     G   (2.*DY)) + ((Z(I,J,NOW) + Z(I-1,J,NOW))/(2.*DY))))                   RNP 78
  10 CONTINUE                                                                 GHN 78
CC
CC
CC       THE FOLLOWING IS AN OUTPUT ALGORITHM                                RNP 78
CC
CC
      IF(T.LT.TWRITE) GO TO 50                                                RNP 78
      IF(NOW.NE.2) GO TO 30                                                   GHN 78
      IF(JFLAG.EQ.0) GO TO 1?                                                 RNP 78
      PRINT*,((" DISPL Z(CELL ",K,")= ",Z(K,JWRITE,NOW)),K=2,IMAX)            RNP 78
   1  IF(IFLAG.EQ.0) GO TO 15                                                 RNP 78
      PRINT*,((" DISPL Y(CELL ",K,")= ",Y(K,JWRITE,NOW)),K=2,JMAX)            RNP 78
```

```
15    DO 21 I=1,100
      DO 21 J=1,21
   21 AL(I,J)=" "
      DO 22 J=1,21
   22 AL(1,J)="I"
      DO 23 I=2,98
   23 AL(I,11)="-"
      AL(2,1)="1"
      AL(3,1)="."
      DO 25 J=3,19,2
   25 AL(3,J)="."
      AL(4,3)="8"
      AL(4,5)="6"
      AL(4,7)="4"
      AL(4,9)="2"
      AL(4,11)="0"
      AL(4,13)="2"
      AL(4,15)=","
      AL(4,17)="6"
      AL(4,19)="8"
      AL(3,21)="1"
      AL(4,21)="."
      DO 26 J=13,21,2
   26 AL(2,J)="-"
      SCALE=0.0
      DO 27 I=1,IMAX
      TEST=AMAX1(ABS(Y(I,JWRITE,NOW)),ABS(Z(I,JWRITE,NOW)))                    RNP 78
   27 IF(TEST.GT.SCALE) SCALE=TEST
      IF(SCALE.EQ.0.0) SCALE=1.0
      ZWRITE = (JWRITE- 2 ) * DZ                                               RNP 78
      PRINT 101,T,SCALE,DY,ZWRITE                                              RNP 78
  101 FORMAT(///," TIME(SEC) = ",F6.4,", SCALE(CM) = ",E12.3,", DY(CM) = "     RNP 78
     $ ",E12.3,", OUTPUT DEPTH Z(CM) = ",E12.3,///)                            RNP 78
      DO 28 I=1,IMM
```

```
      L=I+1                                                          RNP 78
      IF(RPLOT.EQ.0) GO TO 275                                       RNP 78
      JY=11.5-10.*Y(L,JWRITE,NOW)/SCALE
      IF(JY.LT.1) JY=1
      IF(JY.GT.21) JY=21
      AL(I,JY)="Y"
  27  JZ=11.5-10.*Z(L,JWRITE,NOW)/SCALE                              RNP 78
      IF(ZPLOT.EQ.0) GO TO 28                                        RNP 78
      IF(JZ.LT.1) JZ=1
      IF(JZ.GT.21) JZ=21
      AL(I,JZ)="Z"
      IF(JY.EQ.JZ) AL(I,JY)="X"
  28  CONTINUE
      DO 2  K=1,10
      T=10* K
  2   AL(I,11)="0"
      AL( ,11)="1"
      AL(1 ,11)="2"
      AL(2 ,11)="3"
      AL(3 ,11)="4"
      AL(4 ,11)="5"
      AL(5 ,11)="6"
      AL(6 ,11)="7"
      AL(7 ,11)="8"
      AL(8 ,11)="9"
      AL(9 ,11)="1"
      AL(99,11)="0"                                                  SHN 78
```

```
C                                                                       RNP 78
C        LOCSHOK IS THE LOCATION OF SHOCK FRONT ON THE GROUND FOR PLOT  RNP 78
C        YYSHOCK= 0 IMPLIES HORIZONTAL CELL 2, WHICH IMPLIES AL(1,J)    RNP 78
C
      LOCSHOK =(YYSHOCK + (DY/2))/DY + 1                                RNP 78
      AL(LOCSHOK,1) = "A"                                               RNP 78
      AL(LOCSHOK,2) = "B"                                               RNP 78
      DO 29  J=1,21                                                     GHN 78
   29 PRINT 102,(AL(I,J),I=1,IMAX)
  102 FORMAT(1X,100A1)
   30 CONTINUE
CC
CC
      LAST = NOW
      NOW = NEXT
      NEXT = 6 - LAST - NOW
      T = T + DT                                                        GHN 78
      IF (TMAX-DY/VEL - (T-TZERO)) 20,20,5                              RNP 78
   20 CONTINUE                                                          GHN 78
      END
```

LIO REFERENCE MAP (R=1)

AL

```
      FUNCTION PRESS(YIELD,HOB,T,YY,RZERO,YYSHOCK)
C
C
C        T = 0 IS  TIME OF BURST
C        CMTOKFT IS CM TO KILOFEET CONVERSION                              RNP 78
C        CMTOMLE = CM TO MILE CONVERSION
C        SLTRANG = SLANT RANGE
C        TARR = TIME OF ARRIVAL OF AIR SHOCK (DNA 3781F PG 193)            RNP 78
C        TPLUS = DURATION OF POS. OVERPRESSURE(GLASSTONE OR BRODE)         RNP 78
C        RZERO IS GROUND RANGE AT WHICH IT IS DESIRED TO START PROBLEM:
C              R NOT EQUAL ZERO NEGATES ALL PRESSURE IMPULSE PRIOR TO      RNP 78
C              RZERO: USE IN CONJUNCTION WITH PROPER TZERO                 RNP 78
C        PSITODC = PSI TO DYNES/CM**2 CONVERSION                           RNP 78
C
C
CCCC
CCCC      CONSTANTS
CCCC
      IF(YY.LT.RZERO) GO TO 1
      CMTOKFT = 3.28E-5
      PSITODC = 6.893E4
      SLTRANG =((HOB**2 + YY**2)**0.5)*(CMTOKFT)
CCCC
CCCC      BEGIN TO CALCULATE PARAMETERS FOR PRESS1
CCCC
CC
CC        TARR BY BRODE(DNA 3781F) FOR PRESS1
CC
      TARR = 1.E-3*(.54291*(YIELD*1000.)-(21.185*SLTRANG)*((YIELD*1000.)
     $ **.667) + 381.8*(SLTRANG**2)*((YIELD*1000.)**.333) + 2383.*
     $(SLTRANG**3))/((YIELD*1000.)**.667 + 2.048*SLTRANG*((YIELD*1000.)
     $ **.333) + 2.6872*(SLTRANG**2))
      IF(YY.EQ.0.0) GO TO 5
      IF(HOB/YY.GE.1.) GO TO 5                                           RNP 78
C
```

```
C        TARR2 = SAME AS TARR EXCEPT USE 2000 IN PLACE OF 1000
C
 4     TARR2= 1.E-3*(.5291*(YIELD*2000.)-(21.185*SLTRANG)*((YIELD*2000.)
     $ **.667) + 361.8*(SLTRANG**2)*((YIELD*2000.)**.333) + 2383.*
     $(SLTRANG**3))/((YIELD*2000.)**.667 + 2.048*SLTRANG*((YIELD*2000.)
     $ **.333) + 2.3872*(SLTRANG**2))
       IF(YY.EQ.0.0) GO TO 5
       TARR = TARR*HOB/YY + TARR2*(1.-HOB/YY)                          RNP 78
 5     CONTINUE
C
C
C        YYSHOCK = LOCATION OF SHOCK FRONT ON GROUND
C
       IF((TARR-T).LE.1.E-4) YYSHOCK = YY
       IF (T.LT.TARR ) GO TO 1
C
C        PEAKP = PEAK OVERPRESSURE (GLASSTONE FIT)
C
       YYF =  YY*CMTOKFT*1000
       IF(YYF.GT.2304.) GO TO 810
       IF(YYF.GE.1200.) GO TO 800
       IF(YYF.GE.1050.) GO TO 780

       IF(YYF.GE.0725.) GO TO 770
       PEAKP = (14.-36.25)/725. * (YYF) + 36.25
       GO TO 3
 770   PEAKP = (17.-14.)/(1050-725.)*(YYF-725.) + 14.
       GO TO 3
 780   PEAKP = ((3.-17.)/(1500.-1050.))*(YYF-1050) + 17.
       GO TO 3
 800   PEAKP = ((2.5-3.)/(2500.-1500.))*(YYF-1500.) + 9.
       GO TO 3
 810   PEAKP = 0.0
 3     CONTINUE
```

```
C
C        TPLUS IS LINEAR FIT TO GLASSTONE FOR PARTICULAR YIELD
C
C
      TPLUS = ((.33-.15)/(2500.))*YYF + .15
 10   CONTINUE
CCCC
CCCC     P(T) =PRESS1 = NICKEL (52 GLASSTONE)
CCCC
      AM=1.+.342*ALOG(PEAKP)-.136*(ALOG(PEAKP))**2.+.025*(ALOG(PEAKP))**
     $3.
      TAU = (T-TARR)/TPLUS
      IF(TAU.GT.1.) GO TO 1
      PRATIO = 1. - (1. - (1. - TAU)**AM)**(1./AM)
      PRESS = PEAKP*PRATIO
      IF(PRESS.LT.0.) GO TO 1
      PRESS = PRESS*PSITOO
      GO TO 90
 1    PRESS = 0.0
 90   RETURN
      END
```

Appendix G

Estimate of Apparent Airshock Velocity Along Ground Surface

The shock front from a nuclear burst can be considered a spherical shell which is expanding with some average velocity, V_{ave}. The intersection of this spherical shock front with the ground surface forms a circular region. This circular line of intersection will expand along the ground with a velocity, called the apparent velocity V_{app}, which will differ from V_{ave}. If the airshock is approximated locally as a planar wavefront, the following figure describes the position of the airshock at two times, t and t+dt.

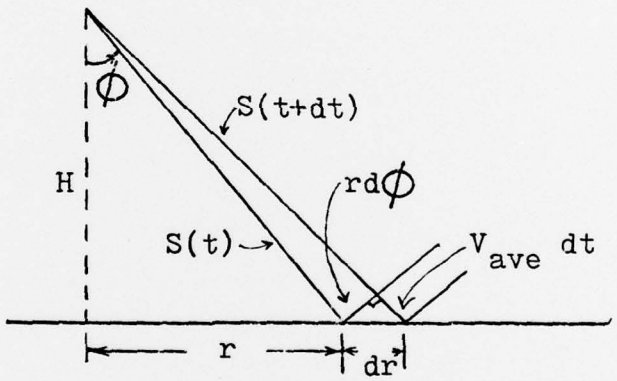

In dt, the shock wave radius S (also equal to the slant range) expands by Vavedt. Thus,

$$S(t+dt) = S(t) + V_{ave}dt.$$

Also,

$$(dr)^2 = (V_{ave}^2\ dt)^2 + \left[S(t)\ d\phi \right]^2 , \text{ or}$$

$$\frac{dr^2}{dt} = V_{ave}^2 + \left[S(t)\ \frac{d\phi}{dt} \right]^2 .$$

But, $\tan\phi = \frac{r(t)}{H}$ and $\sec\phi = \frac{S(t)}{H}$.

Also, $\frac{d}{dt}(\tan\phi) = \sec^2\phi \frac{d\phi}{dt} = \frac{1}{H}\frac{d\,r(t)}{dt}$.

which gives $\frac{d\phi}{dt} = \frac{1}{H\sec^2} \frac{d\,r(t)}{dt}$

$$= \frac{1}{H}\left(\frac{H}{S(t)}\right)^2 \frac{d\,r(t)}{dt} = \frac{H}{S^2(t)} V_{app} .$$

Substituting for $\frac{d\phi}{dt}$ in the expression for $\frac{dr}{dt}$ above yields

$$\left(\frac{dr}{dt}\right)^2 = V_{app}^2 = V_{ave}^2 + \left[S(t) \frac{H V_{app}}{[S(t)]^2} \right]^2 ,$$

or $$V_{app}^2 \left[1 - \frac{H}{S(t)} \right]^2 = V_{ave}^2 .$$

Solving for V_{app},

$$V_{app} = \left\{ \frac{V_{ave}^2}{1 - \left(\frac{H}{S(t)}\right)^2} \right\}^{\frac{1}{2}} .$$

Finally substituting for $S(t) = \left[(H^2 + (r(t))^2 \right]^{\frac{1}{2}}$,

$$V_{app} = \left\{ \frac{V_{ave}^2}{1 - \frac{H^2}{H^2 + r^2}} \right\}^{\frac{1}{2}} .$$

Vita

Richard N. Price was born on 4 January 1951 - Jackson, Mississippi. Graduating from high school in Jackson in 1969, he entered Mississippi State University. Upon completing the degree requirements for a Bachelor of Arts degree in Physics and being commissioned into the USAF through the ROTC program in August 1973, he entered active duty that September. His entire Air Force career has been spent at Wright-Patterson Air Force Base, Ohio, first serving as microelectronics technical analyst at the Air Force Foreign Technology Division and then entering the Air Force Institute of Technology's School of Engineering in June 1977.

Permanent mailing address: Route 1, Box 22M
Terry, Mississippi 39170

UNCLASSIFIED

SECURITY CLASSIFICATION OF THIS PAGE (When Data Entered)

REPORT DOCUMENTATION PAGE		READ INSTRUCTIONS BEFORE COMPLETING FORM
1. REPORT NUMBER AFIT/GNE/PH/78D-21	2. GOVT ACCESSION NO.	3. RECIPIENT'S CATALOG NUMBER
4. TITLE (and Subtitle) The Nuclear Airshock Precursor: A Study of the Contribution of Airblast-Induced Seismic Waves		5. TYPE OF REPORT & PERIOD COVERED MS Thesis 6. PERFORMING ORG. REPORT NUMBER
7. AUTHOR(s) Richard N. Price Capt		8. CONTRACT OR GRANT NUMBER(s)
9. PERFORMING ORGANIZATION NAME AND ADDRESS Air Force Institute of Technology (AFIT/EN) Wright-Patterson AFB, Ohio 45433		10. PROGRAM ELEMENT, PROJECT, TASK AREA & WORK UNIT NUMBERS
11. CONTROLLING OFFICE NAME AND ADDRESS		12. REPORT DATE December 1978 13. NUMBER OF PAGES
14. MONITORING AGENCY NAME & ADDRESS(if different from Controlling Office)		15. SECURITY CLASS. (of this report) Unclassified 15a. DECLASSIFICATION/DOWNGRADING SCHEDULE

16. DISTRIBUTION STATEMENT (of this Report)

Approved for public release; distribution unlimited

17. DISTRIBUTION STATEMENT (of the abstract entered in Block 20, if different from Report)

18. SUPPLEMENTARY NOTES

Approved for public release; IAW AFR 190-17

Joseph P. Hipps, ~~Major~~, USAF
Director of Information 19 Jan 79

19. KEY WORDS (Continue on reverse side if necessary and identify by block number)

Airblast-induced seismic waves
Nuclear airshock precursor

20. ABSTRACT (Continue on reverse side if necessary and identify by block number)

The coupling into the ground of airblast energy from an atmospheric nuclear burst is postulated as a mechanism which may contribute to if not independently cause the observed airshock precursor. A computer model to test the hypothesis is constructed by assuming an elastic ground medium, applying finite difference techniques to the equations of motion, and using the space- and time-varying overpressure from the nuclear burst to induce the

DD FORM 1 JAN 73 1473 EDITION OF 1 NOV 65 IS OBSOLETE

UNCLASSIFIED

SECURITY CLASSIFICATION OF THIS PAGE (When Data Entered)

seismic motions within the ground.

The surface velocities resulting from simulation of a 28 kiloton atmospheric burst at 500 feet height of burst yielded a dust layer ballistically reaching only 0.64 cm at its highest point for the stiff one-layer ground medium, 0.096 cm for the softer one-layer medium, and a negligible height for the more realistic four-layer Frenchman Flats medium. Thus, the airblast-induced precursor as postulated (ballistic rise only) fails to re-create the 2 - 3 meter high dust layers observed in experimental atmospheric nuclear testing. However, the motions are felt to be significant enough to be included in any attempt to model from first principles the precursor and the up-sweep of dust behind the shock front.